

Shanghai Jiao Tong University

University of Michigan - Shanghai Jiao Tong University Joint Institute

Cyber-Physical Systems for Smart Grid

by

Yibo Pi

A thesis submitted in partial satisfaction of the
requirements for the degree of Master of Science in
Electrical and Computer Engineering at Shanghai Jiao Tong University

Committee in charge:
Prof. Xudong Wang, Chair
Prof. Jun Zhang
Prof. Xinen Zhu

Shanghai
Jan., 2015

Abstract

This thesis provides a complete framework for integrating photovoltaic systems (PVs) and electric vehicles (EVs) into the residential distribution grid. In the framework, the distribution grid and communication networks are tightly coupled together and constitute a tightly-coupled cyber-physical system (CPS). From the relation between power grid and communication networks, we can gain insights about building other CPSs for smart grid and provide a systematic guideline for the design of communication networks in smart grid applications.

In the first research topic, the problems of integrating PVs into the distribution grid are considered. With the increasing number of residential PV systems, the maximum power point tracking (MPPT) used in traditional PV systems induces physical problems to the existing distribution grid and fairness problems among PV systems. To solve the above problems, coordinated power point tracking (CPPT) is proposed, where a central controller coordinates the power points of PV systems via a wireless network. The objective of the coordination is to maximize the output power of PV systems under the physical constraints of voltage, power flow and fairness. An optimization problem is first formulated and the optimal condition for the optimization problem is derived. Based on the optimal condition, a practical distributed scheme is developed and a hierarchical wireless mesh network (WMN) is designed to satisfy delay requirements. Extensive simulation results show that CPPT outperforms MPPT.

In the second research topic, the problems of integrating EVs into the distribution grid are considered. The integration of EVs in high penetration levels induces physical problems including low-voltage and transformer overload and the fairness problem among EVs. Since EVs only have on/off states, fairness among EVs is achieved by operating the on/off states of EVs. Fair queueing theory is used to determine when and which EVs should be turned on/off. The EV charging system is first mapped to a fair queueing system. Under the system, the ideal discipline, physical multi-server generalized processor sharing (pMGPS), is first studied. Because the pMGPS assumes that EVs have continuous charging powers, a packetized fair queueing scheme for EV charging (SFC) is then designed, which can achieve the nearly perfect fairness performance at the sacrifice of power grid capacity utilization. To overcome the drawbacks of SFC, an enhanced scheme, SFC+, is designed to better utilize the power grid capacity. The fairness performance of both SFC and SFC+ are rigorously proved. Besides, the total energy EVs are charged under the SFC+ is proved to be as good as that under the pMGPS, which implies that the SFC+ approximates the ideal pMGPS discipline.

Contents

1	Introduction	3
1.1	Power Point Tracking for Photovoltaic Systems	4
1.2	Electric Vehicle Charging in the Distribution Grid	7
2	Network Coordinated Power Point Tracking for Photovoltaic Systems	13
2.1	System Architecture	13
2.2	Optimal Power Point Tracking for PV systems	15
2.2.1	Optimal Solution and Its Limitations	18
2.2.2	Conditions on Optimal Power Points	19
2.3	A Practical Distributed Scheme	25
2.3.1	Surplus power allocation algorithm	25
2.3.2	Power curtailment in a PV system	25
2.3.3	Procedures of CPPT	27
2.4	Network Design	27
2.4.1	Mesh Network Architecture for CPPT	29
2.4.2	Protocol Design	30
2.5	Performance Evaluation	35
2.5.1	Experiment Setup	37
2.5.2	Physical system evaluation	37
2.5.3	Relation Between Communication Delay and CPPT Performance	40
2.5.4	Performance of the Communication Network	42
2.6	Summary	43
3	A Fair Queueing Scheme for Electric Vehicle Charging	45
3.1	Overall System Design	45
3.1.1	System Architecture	45
3.1.2	General Operations Inside a Sub-Grid	48

3.2	Fair Queueing for EV Charging	50
3.2.1	Mapping EV Charging System into a Queueing System	51
3.2.2	Physical Multi-Server GPS (pMGPS)	54
3.2.3	A Start-Time Fair Queueing Scheme for EV Charging	55
3.3	Fairness Analysis of the SFC	60
3.4	Fairness Analysis of the SFC+	63
3.5	Performance Evaluation	72
3.5.1	Experimental Setup	72
3.5.2	Fairness performance of the SFC and SFC+	73
3.5.3	Total energy charged for EVs under the SFC+ and pMGPS	74
3.6	Summary	75
4	Conclusion	77
4.1	Contributions	78
4.2	Future Work	79
	Acknowledgments	81
	A Publications	83
	Bibliography	88

List of Figures

1.1	A distribution grid with PV systems	5
2.1	The major components in a sub-grid	15
2.2	Thevenin equivalent circuit for the port between i and the ground	20
2.3	Relationship among $V_i, V_{Th}, V_{max}, V_{min}$	21
2.4	Phase relationship between V_i and ΔV_i	23
2.5	Thevenin equivalent circuit for the port between i and j	24
2.6	Illustration of two over-voltage cases	27
2.7	Timing relationship of messages between the central controller and inverters	28
2.8	Two-layer hierarchical WMN for CPPT	29
2.9	Communication network topology in experiments	37
2.10	Performance of MPPT-based schemes.	38
2.11	Performance of a CPPT scheme.	38
2.12	Performance of different schemes at different voltages	39
2.13	The number of over-voltage occurrence at different delays	41
3.1	The major components in a sub-grid	46
3.2	The major components in a sub-grid	47
3.3	Voltage variations under periodic control and no control on EVs	48
3.4	Illustration of the two multi-server queueing systems with queue preference	52
3.5	A toy example about how SFC works	56
3.6	Physical topology of sub-grid used in experiments	72
3.7	Worst-case bounds of fairness measure under the SFC	73
3.8	Total energy charged for EVs under the SFC, SFC+ and pMGPS schemes when sub-grid capacity is constrained by voltage and transformer capacity respectively.	75

List of Tables

2.1	Jain index under different transformer voltage levels	39
2.2	Over-voltage times and average rounds of CPPT in a day	40
2.3	Four parameters of the reverse power flow with respect to round-trip delay . . .	40
2.4	Fairness versus communication delay	41
2.5	Communication delay under different channel conditions	42
2.6	Communication delay under different channel conditions	42
3.1	Bounds of fairness measure under the SFC+	74

Chapter 1

Introduction

Smart grid is believed to be the future of power grid, which aims at using modernized communication technology to smarten existing power grid. The applications in smart grid involves monitoring, management and control. All three functions need communication technology for information collection and dissemination. However, to date only limited communication technologies have been widely accepted in smart grid communications and most of these technologies are wired. To leverage the advantages of communication networks for smart grid, especially wireless networks, communication networks should be designed to satisfy the requirements of applications in smart grid. To understand the requirements of the applications on communication networks, the integration of photovoltaic systems (PVs) and electric vehicles (EVs) in power grid is considered. Moreover, considering the diversity of applications, the design of communication networks is usually application-specific. We want to develop a systematic approach to guide the design of communication networks based on the framework of cyber-physical system (CPS).

In the framework of CPS, the CPSs are categorized into loosely-coupled CPS and tightly-coupled CPS. In a CPS view, all applications with CPSs in smart grid can be classified into two types. Simply speaking, the applications that monitor and manage the power grid belong

to the loosely-coupled CPS regime, while the applications that control the power grid belong to the tightly-coupled CPS regime, where physical systems cannot operate without the help of communication networks. This classification reflects the relation between power grid and communication networks. Through this relation, we can develop general procedures to provide a guideline for the design of communication networks in smart grid. In this thesis, it can be seen that the integration of PVs and EVs into power grid belongs to the tightly-coupled CPS regime. A complete framework is developed for the integration of PVs and EVs, which can be easily extended to other cyber-physical systems in smart grid.

In the rest of this chapter, the background and motivations of the research on the integration of PVs and EVs are presented.

1.1 Power Point Tracking for Photovoltaic Systems

Photovoltaic cells have been studied to harness solar energy for decades of years. Continuing breakthroughs in solar cell improve its efficiency up to 40% (Green et al., 2012) and now PV cells with average efficiency up to 20% have been commercialized (Song et al., 2012). The increasing efficiency and decreasing price of solar cells greatly thrust the installation of distributed PV resources into the distribution grid to generate electricity for daily use. Since PV cells generate dc voltage, an inverter is needed to invert dc voltage into ac to synchronize with the grid. The combination of an inverter and its controlled PV cells is called a PV system. The inverter controls the power point of PV cells using the maximum power point tracking (MPPT) algorithm (Esrām and Chapman, 2007). The algorithm ensures PV cells always working at the maximum power point so as to inject the maximum power into the grid, while the side effects of this power injection are the over-voltage problem, i.e., the voltage of users exceeds prescribed range, and the reverse power flow problem, i.e., power flows into the grid exceeds allowed level.

The over-voltage problem is ascribed to the voltage rise phenomenon induced by injecting

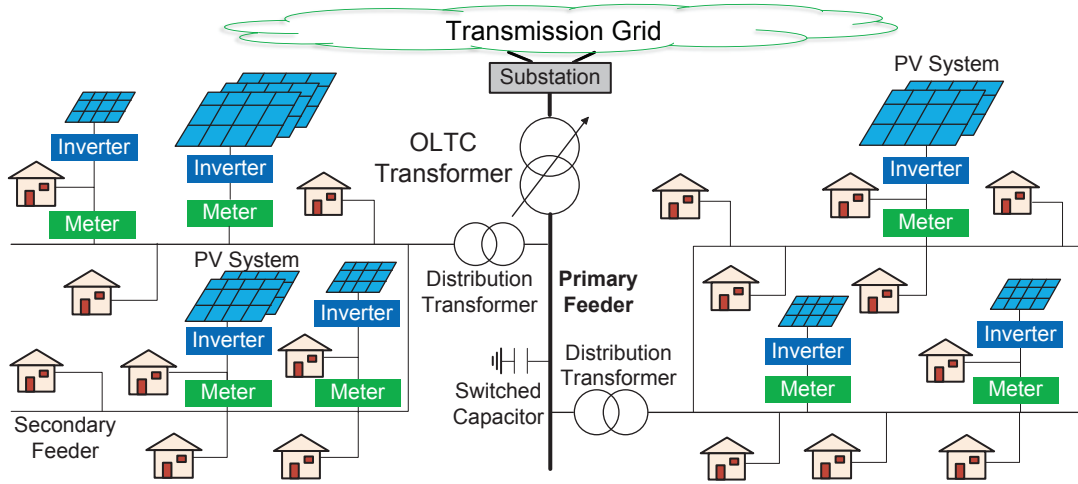


Figure 1.1: A distribution grid with PV systems

active power into the grid. Along with voltage rise is reverse power flow. In traditional distribution network, the direction of power flow is from substation to the downstream primary feeders and from the secondary feeders to users as in Figure 1.1. The integration of PV systems changes the power flow reversely from end users to the secondary feeders and in high penetration case, from the secondary feeder to the primary feeder, interfering the operations of network devices. Voltage rise also induces fairness problem. Since the severity of voltage rise on users differs with their positions on transmission line, PV systems of some users can inject more power into grid than those of other users. As users can benefit from injecting power into grid, unfair chances for power injection implies unfair benefits.

To solve these problems, we propose a coordinated power point tracking (CPPT) mechanism, which aims to maximize the benefits of users under the constraints of voltage, power flow and fairness. The key components of CPPT includes a central controller that centrally manages the power points of PV systems, a wireless network that collects and disseminates information and a local controller inside the inverters of PV systems to ensure the voltage of users. In general, CPPT includes two steps: 1) The central controller determines the power points of PV systems based on the status of PV systems. 2) The new power points are sent to inverters via the

communication network. To obtain an optimal two steps should be repeated until the CPPT converges Extensive simulations have been conducted to evaluate the performance of CPPT, which demonstrates that CPPT outperforms MPPT.

There are related work in the literature. Power curtailment in (Esrasm and Chapman, 2009; Wang et al., 2012) is a local method in regulating voltage, which does not need a communication network or knowledge of grid topology, as an inverter simply reduces output power of a PV system once over-voltage is detected. However, neither the reverse power flow nor fairness problem is considered in a local power curtailment method. The droop-controlled inverters in (Tonkoski et al., 2011; Anand et al., 2013) can achieve both voltage regulation and proportional power sharing, but the reverse power flow problem is not considered either. The theoretical work in (DallAnese et al., 2013; Lam et al., 2012) provide distributed solutions to optimal power flow, which can be utilized to control the reverse power flow. However, how to apply these schemes to a practical system remains an open problem. Furthermore, both droop-controlled inverters and the schemes of distributed optimal power flow need admittance matrix of the distribution grid, which is difficult to obtain in practice.

Besides the distributed schemes, many centralized schemes have also been proposed in the literature. In (Liew and Strbac, 2002), an OLTC-based method is proposed to maximize the reverse power flow by adjusting the tap position of on-load changer transformer (OLTC) so that energy generated by PV systems can be maximally utilized. The over-voltage and fairness problems are addressed in (Yoshida et al., 2008), where energy storage system is utilized to store surplus power so that the power generation efficiency among all users is equal. In all these centralized schemes, the reverse power capacity of transformers (Cipcigan and Taylor, 2007) is neglected.

This chapter represents details for coordinated power point tracking (CPPT). In Section 2.1, the system architecture of CPPT is presented. The optimization problem that determines power points of PV systems is formulated in Section 2.2. A practical distributed scheme is

developed in Section 2.3 to track power points of all PV systems. The WMN for CPPT is designed in Section 2.4. Simulations and performance results are reported in Section 2.5. The chapter is concluded in Section 2.6.

1.2 Electric Vehicle Charging in the Distribution Grid

Electric vehicles (EVs) have been considered as an alternative to conventional vehicles. It has been forecasted that by 2050, the penetration level of EVs will reach 62% in (Balducci, 2008). Compared to charging at public charging stations, charging at home is attractive to EV users, because it is readily available. EV users can have their EVs charged immediately after they arrive home. However, unlike public charging stations that are deliberately designed to charge EVs, charging EVs at high penetration levels at homes put a threat to the existing residential distribution grid.

EV charging rates are much higher than the rated powers of home appliances such as air conditioners and heaters. For individuals, charging an EV at home can be easily achieved by installing a higher-powered outlet or a home charging station. However, from the perspective of distribution grid operators, if a large number of EVs require to be charged at the same time, a new peak load will be induced, which is much higher than the peak load induced by home appliances. According to IEEE Standard C57.92, the capacity of existing transformers is selected based on peak load. The new peak load induced by EVs will overload existing transformers and reduce their lifetime. In addition to the transformer overload problem, EV charging increases the current flowing through transmission feeders and results in more severe voltage drop along these feeders, especially in rural areas where users locate sparsely and are connected by long transmission feeders (Short, 2004). Voltage drop beyond prescribed operation range induces the undervoltage problem, which may cause damages to home appliances.

The above two physical problems indicate that capacity of the existing distribution grid

is limited. EV users have to compete for the limited capacity on several aspects, which may include the sequence of charging, the charging rate and charging time. Allocation of these limited resources should reflect the need of EV users; otherwise, the quality of charging service is poor to EV users. To charge EVs while avoiding the above physical problems and ensuring quality of charging service, there are generally three solutions. The first solution is to reinforce the existing distribution grid until its capacity exceeds the new peak load. Due to the large number of EVs and their high charging rates, the new peak load is extremely high, which results in the reinforcement costly.

Under the observation that EV users have different charging requirements, there is no need to charge EVs immediately after their arrivals. The second solution is to schedule the charging of EVs so that the safety of the distribution grid is ensured and the charging requirements of EV users are satisfied. The key idea of scheduling is shifting EV charging from peak time to non-peak time to reduce the stress of distribution grid. In (Clement-Nyns et al., 2010), the charging requirements of EV users are said to be satisfied if the required energy of EV users is charged before deadlines. Under the assumption that the distribution grid capacity is enough, an optimization problem is formulated to minimize power losses based on the forecasted load profiles of users. Because it is impossible to exactly forecast the load profile, a stochastic programming is then proposed in (Clement-Nyns et al., 2010) to handle the forecasting errors. Even so, the forecasted load profile may still differ a lot with the real load profile, especially when the number of users being forecasted is small. In this case, the charging decisions based on the forecasted load profile will result in a severe violation of the physical constraints. The same problem of using historical or forecasted data for EV charging can be found in (Sundstrom and Binding, 2012; Sortomme et al., 2011; Deilami et al., 2011).

Besides the problems induced by the forecasted errors, the above methods do not consider the unfairness among EV users due to early departure. For EV users having the same energy requirement, each of them prefers to be charged first with maximum charging rate and maximum

charging time so that the charging process can be finished early in case of early departure before the charging deadline. Thus, allocating more power to some EV users than the others induces the fairness problem and charging EVs without efficiently utilizing the limited capacity induces the efficiency problem. Unless the distribution grid is reinforced so that EVs can be charged as home appliances, the fairness and efficiency problems always exist.

A simple method to solve the above three problems and the energy requirements as a whole is to reinforce the existing distribution grid. The cost of reinforcement depends on the energy requirements of EV users. If EV users require that EVs be charged immediately after they are plugged in just like normal home appliances, an extremely high peak load will be induced, especially when the new peak load induced by EVs coincides with the peak load induced by home appliances after users arrive home. The distribution grid needs transformers with much larger capacity and feeders with much lower impedance to support the extreme peak load, which are very costly. Considering the cost of reinforcement and the forecasted errors, authors in (Ardakanian et al., 2013; Yoshida et al., 2008) propose to proportionally share the distribution grid capacity among EVs. However, the distribution grid capacity required in the above two papers is difficult to be accurately obtained, especially when voltage is the active constraint (Richardson et al., 2012). Furthermore, the proportional sharing requires EV chargers to support a continuous charging rate, while the commercial chargers are designed to charge EVs only at rated powers.

Since the above problems are concerned with EVs in the same distribution grid, these EVs should be coordinated for charging. A framework for charging EVs in the residential distribution grid is developed in this paper, where a central controller coordinates the charging rates of EVs via a communication network. The general coordination process includes three simple steps: 1) The central controller collects the data of the distribution grid state. 2) Based on the collected data, the central controller determines the on/off states of EVs. 3) The on/off states are disseminated to EVs. The data collection and charging rates dissemination are accomplished

by the communication network. However, there exist several challenging issues.

The first issue is to design a scheme for the central controller to determine the on/off states of EVs. The scheme should efficiently and fairly utilize the limited distribution grid capacity to charge EVs within the physical constraints including voltage operation range and transformer capacity. An efficient use of the capacity makes the distribution grid operate at the margin of the physical constraints. The distribution grid is very susceptible to load fluctuations and the erroneous charging decisions made by the charging scheme, which may result in a violation of the physical constraints. The erroneous charging decisions are made based on the inaccurate data of the distribution grid state. To ensure the stability of the distribution grid, the real-time data of the distribution grid state should be collected. A safety margin should be reserved to tackle the load fluctuations and the real-time data of distribution grid state should be collected for making scheduling decisions. Even so, it is still possible that the physical constraints may be violated and we need to consider the cases when the physical constraints are violated. According to IEEE Std C57.92 and 1250, the violations of the physical constraints should be solved within tolerable time depending on the severity of the violations. Thus, the second issue is to design system parameters like the safety margin to ensure the probability of undervoltage is below expected level.

The above two issues are addressed in this paper as follows. The EV charging system in the distribution grid is first mapped to a fair queueing system. Based on the system, a physical multi-server GPS (pMGPS) scheme is first proposed, which can allocate power among EVs fairly and efficiently utilize the power grid capacity. However, the pMGPS assumes EVs have continuous charging powers. We need to design a packetized fair queueing scheme that schedules the charging of EVs by operating on their on/off states. The packetized fair queueing scheme achieves max-min fairness based on the reference system, named simulated MGPS. There are two packetized fair queueing schemes, SFC and SFC+. The SFC can achieve the fairness performance of one packet difference compared to the sMGPS, but it cannot fully utilize

the power grid capacity. The SFC+ can fully utilize the power grid capacity at the sacrifice of fairness. The fairness performance of both the SFC and SFC+ is rigorously proved. Moreover, total energy EVs can be charged under SFC+ is proved to be as equal as that under the pMGPS, which demonstrates that the SFC+ can achieve as good performance as the pMGPS.

Chapter 2

Network Coordinated Power Point Tracking for Photovoltaic Systems

2.1 System Architecture

Usually multiple primary feeders are connected to the substation in a distribution grid. However, these primary feeders run independently. Thus, without loss of generality, only one primary feeder is considered in the distribution grid, as shown in Fig. 1.1. The primary feeder is connected to multiple transformers, each of which supports multiple secondary feeders. Through a secondary feeder, a number of users distributed at different locations are connected to the grid. A user may install a PV system that is connected to the grid through an inverter. For a user with a PV system, we assume there exists a smart meter that can measure power usage and voltage of the user. The smart meter can communicate with the inverter to share its measured information via a communication link such as RS-485. To store surplus power for a PV system, a user may have a battery. Suppose the battery is always enough to absorb the surplus power from a PV system, then the PV system works locally and has no interaction with the grid. In this paper, we consider PV systems that send surplus power to the grid. In other words, we

assume no battery is installed or the battery is not enough to store all surplus energy of a PV system. In fact, our assumption is reasonable, because using battery to absorb all surplus power from a PV system demands a large capacity of battery bank, which is expensive in practice. Under our assumption, the battery of a user is considered as part of the load.

Usually output power of a PV system is controlled by an MPPT mechanism in the inverter. However, MPPT results in a few issues. Firstly, over-voltage is not controlled pro-actively. We know that multiple PV systems may make contributions to over-voltage at the same point of the secondary feeders. If the power points of these PV systems are determined in an coordinated way, then over-voltage will occur with a much lower probability. Secondly, the power that flows back to the primary feeder is not controlled. In theory, the reverse operation is doable, but is subject to two constraints: 1) the input voltage level of step-up operation must be controlled strictly within rating to ensure a safe voltage level at the output side; 2) the reverse power flow needs to be controlled so that it does not damage the transformer. As a result, a threshold must be set for the reverse power flow, and the voltage levels at both sides of the transformer must be maintained within rating. Thirdly, the surplus power that can be sent to the grid is not coordinated among different PV systems. Thus, PV systems get unfair share of revenues generated from solar energy. To avoid unfairness, the surplus power allowed in a grid must be fairly allocated to each PV system.

To avoid issues in MPPT, output power control of different PV systems needs to be coordinated. Thus, the focus of this paper is to develop a framework of coordinated power point tracking (CPPT) for grid-connected PV systems. It should be noted that a sub-grid consisting of one transformer and several secondary feeders works independently from another sub-grid. Thus, in this paper, CPPT is studied for a sub-grid instead of the entire distribution grid.

The system architecture that shows the basic operation of CPPT is shown in Fig. 2.1. CPPT demands a central controller to coordinate the power points of all the PV systems. It is co-located with the transformer where a smart meter is also added to work together with

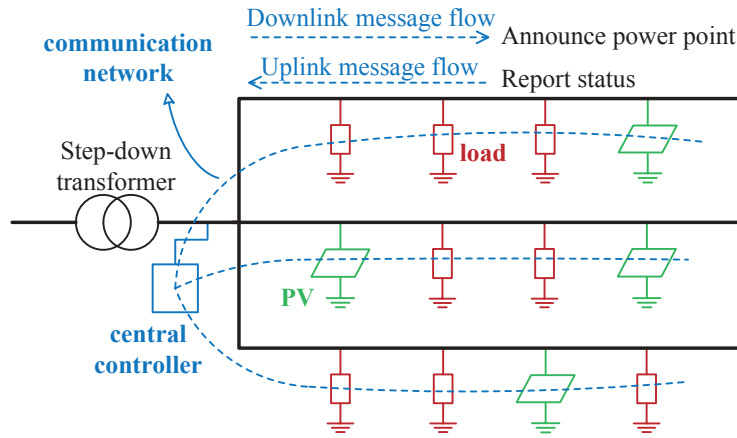


Figure 2.1: The major components in a sub-grid

the central controller. The central controller needs to communicate with all PV systems, so a communication network is needed between the central controller and all PV systems. The communication device is usually co-located with the inverter. Through the communication network, an inverter sends status information (e.g., voltage and power of a user) measured by the smart meter to the central controller. The central controller determines the power point of each PV system and then sends such information back. Once an inverter receives a power point, it executes a power point tracking algorithm to track the output power, and the same power tracking algorithm as that in MPPT can be employed. Since the power point is known to the tracking algorithm, the tracking process converges much faster than the entire process of MPPT. As shown in Fig. 2.1, the central controller and the inverters are connected via a WMN. The reason for using WMN and the design of WMN are addressed in details in Section 2.4.

2.2 Optimal Power Point Tracking for PV systems

Connecting points of users and the transformer in the sub-grid are indexed as follows. The connecting point at the secondary side of the step-down transformer is indexed by 0. The connecting point between a secondary feeder and a user with PV system is indexed from 1 to n . Thus, the set of users with a PV system is $\mathcal{N}_1 = \{1, \dots, n\}$. For users without a PV system,

their points connecting with the secondary feeder are indexed by the set of $\mathcal{N}_2 = \{n+1, \dots, m\}$. Thus, the set of all connecting points in the sub-grid is $\mathcal{N} = \{0\} \cup \mathcal{N}_1 \cup \mathcal{N}_2 = \{0, 1, \dots, m\}$. The admittance between i and j is denoted by y_{ij} , so $\mathbf{Y} = [y_{ij}]_{i,j \in \mathcal{N}}$ is the admittance matrix of the entire sub-grid. Let $\mathbf{V} = [V_0, \dots, V_m]$ be the voltage vector of all connecting points, where $V_i = |V_i| \angle \theta_i$ and θ_i is the phase angle. For a point $i \in \mathcal{N} \setminus \{0\}$, complex power is $S_i = P_i + jQ_i = P_{G_i} - P_{L_i} + j(Q_{G_i} - Q_{L_i})$, where P_{G_i} and Q_{G_i} are the active and reactive power from a PV system, and P_{L_i} and Q_{L_i} are the active and reactive power of load. Currently, a standard PV system only generates active power, so $Q_{G_i} = 0$. For a user without a PV system, both P_{G_i} and Q_{G_i} are zero. Thus, if $P_i > 0$, we know that a PV system i is injecting power to the sub-grid, so P_i is called the *surplus power*.

Objective Function When the output power of all PV systems is maximized, the power pulled from the grid is minimized. Thus, the objective of the optimization problem is to determine the power points of all PV systems such that the power from the grid is minimized. Since only active power is generated in PV systems, the power from grid to be minimized is also active power. As a result, we have the following objective function:

$$\min_{\{\mathbf{P}_G\}} P_0 \quad (2.1)$$

where P_0 is the power pulled from the grid and $\mathbf{P}_G = [P_{G_1}, \dots, P_{G_n}]$ is the vector of powers generated by the n PV systems in the sub-grid.

The variables in the objective function need to satisfy the power flow equation of the sub-grid. Moreover, the objective function needs to consider constraints of voltage, reverse power flow, and fairness.

Power Flow Equation Based on the Kirchhoff law, the power flow equation of the sub-grid can be written as

$$e_i^* \mathbf{V} \mathbf{V}^* \mathbf{Y}^* e_i = S_i, \quad \forall i \in \mathcal{N}, \quad (2.2)$$

where $\{e_i\}_{i \in \mathcal{N}}$ is the standard basis vectors in $\mathbb{R}^{|\mathcal{N}|}$, i.e., it is column vector with all zeros except that the i -th element is 1.

Voltage Constraint To ensure proper operation of the sub-grid, voltages of all users need to be maintained within rating. Given the voltage rating $[V_{\min}, V_{\max}]$, the voltage at each connecting point (except for the transformer side) is constrained as

$$V_{\min} + \Delta_V^{lb} \leq |V_i| \leq V_{\max} - \Delta_V^{ub}, \quad \forall i \in \mathcal{N} \setminus \{0\}, \quad (2.3)$$

where Δ_V^{lb} and Δ_V^{ub} are a small value to keep $|V_i|$ from actually reaching the lower limit V_{\min} and the upper limit V_{\max} .

Since the step-down transformer is connected to grid, so its voltage is assumed to be fixed,

$$|V_0| = V_0^{ref}. \quad (2.4)$$

Reverse Power Flow Constraint The constraint on the reverse power flow serves two purposes. One is to prevent the step-down transformer from being overloaded. The other is to provide a flexible fine-tuning mechanism for the grid company to control the amount of power flow from distributed generators (e.g., PV systems). The constraints can be applied to both active and reactive power. However, in this paper all PV systems only generate active power, so the reverse power flow can only be active power. Thus, the constraint of reverse power flow only applies to the active power. As a result, we have the following constraint:

$$P_0 \geq P_0^{lb}, \quad (2.5)$$

where P_0^{lb} is the lower bound for the power flow from grid, i.e., P_0 . Since the constraint is for reverse power flow, $P_0^{lb} \leq 0$. To protect the transformer, P_0^{lb} must be set to a value much smaller than the power rating of the transformer.

Fairness constraint The surplus power that can be generated by a PV system determines the revenue from this PV system. However, the total surplus power that can be supported by the sub-grid is limited due to constraints of voltage and reverse power flow. Thus, the surplus power must be shared by different PV systems in a fair way. In this paper, we consider a fair allocation strategy according to the size of PV systems. More specifically, the share of surplus power (i.e., P_i) is proportional to the size of the PV panel. In other words, $P_i = k_i c$, where k_i is the size ratio of i -th PV system over all PV systems, and c is the total surplus power. Thus, if a PV system has a larger PV panel, it is allocated with a larger share of surplus power. This strategy is reasonable, because a user with a larger investment potentially receives a higher revenue. Suppose a user's load is P_{L_i} and the maximum output power of its PV system is $P_{G_i}^{\max}$, then the surplus power allocated to this user is limited by $P_{G_i}^{\max} - P_{L_i}$. As a result, the fairness constraint is

$$P_i = \min(P_{G_i}^{\max} - P_{L_i}, k_i c), \quad \forall i \in \mathcal{N}_1, \quad (2.6)$$

$$c \geq 0. \quad (2.7)$$

2.2.1 Optimal Solution and Its Limitations

Without constraints (2.6) and (2.7), the optimization problem is non-convex, which is similar to the optimal flow problem in (Lavaei and Low, 2010). The additional constraints in (2.6) and (2.7) change the non-convex feasible set into a convex one so that the optimal solution can be obtained. Unfortunately, the optimal solution cannot be readily applied to CPPT, for the following reasons:

- The admittance matrix of the entire sub-grid, i.e., \mathbf{Y} is needed, but in fact it is unknown.
- The maximum output power of a PV system, i.e., $P_{G_i}^{\max}$, is unknown, as it depends on the instantaneous operation environment.

However, studying the optimization problem can help us find the conditions under which the optimal solution is achieved. Based on these conditions, we can develop a distributed algorithm to determine the power points of all PV systems.

2.2.2 Conditions on Optimal Power Points

In this section, we first prove several lemmas and then derive the theorem for the optimal conditions.

Lemma 1. If the voltage constraint in Eq. (2.3) is satisfied, then PV systems get their optimal power points either when the reverse power constraint in Eq. (2.5) is reached or when all PV systems generate maximum output power.

Proof. Let P' be the sum of active power consumed by loads and power loss, so $P' = \sum_{i \in \mathcal{N} \setminus \{0\}} P_{L_i} + P_{loss}$. Based on the power balance principle, the active power generated by PV systems plus that pulled from the transformer is equal to the active power P' , so $P_0 + \sum_{i \in \mathcal{N}_1} P_{G_i} = \sum_{i \in \mathcal{N} \setminus \{0\}} P_{L_i} + P_{loss}$. Intuitively, to minimize P_0 , we need to increase P_{G_i} , i.e., the power generated by PV systems. However, increasing P_{G_i} may lead to more power consumption, i.e., higher P' . Nonetheless, as long as the increased power of PV systems is always larger than the increment of P' , then P_0 can be reduced by increasing power of PV systems until the reverse power constraint in (2.5) is reached or all PV systems generate the maximum output power.

To prove that the increased power of PV systems is always larger than the increment of P' , we look into power generation in one PV system and its impact to P' . Considering a PV system at the connecting point i , its increased power is denoted by ΔP_{G_i} . Corresponding to

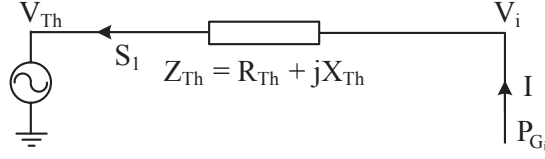


Figure 2.2: Thevenin equivalent circuit for the port between i and the ground

this increased power, the increased power consumption is $\Delta P'$. From point i , the sub-grid can be analyzed via the Thevenin Theorem. As shown in Fig. 2.2, the external circuits for the PV system is replaced by a Thevenin equivalent circuit consisting of a voltage resource V_{Th} and an impedance $Z_{Th} = R_{Th} + jX_{Th}$. Let V_i and I_i be the voltage and current of the PV system. When P_{G_i} increases to $P_{G_i} + \Delta P_{G_i}$, voltage V_i and I_i become $V_i + \Delta V_i$ and $I_i + \Delta I_i$ respectively. Due to the increased current, the increased power consumption $\Delta P'$ is

$$\begin{aligned} \Delta P' &= R_{Th}(|I_i + \Delta I_i|^2 - |I_i|^2), \\ &\leq R_{Th}|\Delta I_i|(|I_i| + |I_i + \Delta I_i|), \\ &\leq 2R_{Th}|\Delta I_i| \max(|I_i|, |I_i + \Delta I_i|). \end{aligned} \quad (2.8)$$

Since $\Delta I_i = \frac{\Delta V_i}{Z_{Th}}$ and $I_i = \frac{V_i - V_{Th}}{Z_{Th}}$, Eq. (2.8) becomes

$$\Delta P' \leq 2 \frac{R_{Th}}{|Z_{Th}|} \left| \frac{\Delta V_i}{Z_{Th}} \right| \max(|V_i + \Delta V_i - V_{Th}|, |V_i - V_{Th}|). \quad (2.9)$$

From the Thevenin equivalent circuit, we know that $V_i = V_{Th} + Z_{Th} \frac{P_{G_i}}{V_i}$ and $V_i + \Delta V_i = V_{Th} + Z_{Th} \frac{P_{G_i} + \Delta P_{G_i}}{V_i + \Delta V_i}$. Thus, we have

$$\left| \frac{\Delta V_i}{Z_{Th}} \right| = \left| \frac{\Delta P_{G_i} V_i - P_{G_i} \Delta V_i}{(V_i + \Delta V_i) V_i} \right| \leq \frac{\Delta P_{G_i} |V_i| + P_{G_i} |\Delta V_i|}{|V_i + \Delta V_i| |V_i|}.$$

In other words, ΔP_{G_i} satisfies

$$\Delta P_{G_i} \geq \left| \frac{\Delta V_i}{Z_{Th}} \right| \left(|V_i + \Delta V_i| - \frac{P_{G_i} |Z_{Th}|}{|V_i|} \right). \quad (2.10)$$

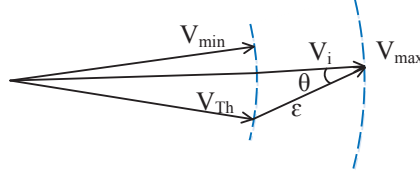


Figure 2.3: Relationship among V_i , V_{Th} , V_{max} , V_{min}

Since $P_{G_i}|Z_{Th}| = |V_i| |V_i - V_{Th}|$, so Eq. (2.10) can be written as

$$\Delta P_{G_i} \geq \left| \frac{\Delta V_i}{Z_{Th}} \right| (|V_i + \Delta V_i| - |V_i - V_{Th}|). \quad (2.11)$$

Considering Eq. (2.9) and Eq. (2.11) together, we get

$$\frac{\Delta P'}{\Delta P_{G_i}} \leq 2 \frac{R_{Th}}{|Z_{Th}|} \frac{\max(|V_i + \Delta V_i - V_{Th}|, |V_i - V_{Th}|)}{|V_i + \Delta V_i| - |V_i - V_{Th}|}. \quad (2.12)$$

We know that $R_{Th} \leq |Z_{Th}|$. Moreover, $|V_i + \Delta V_i| \geq V_{min}$ and the upper bounds of $|V_i - V_{Th}|$ and $|V_i + \Delta V_i - V_{Th}|$ are the same. Define ϵ to be the upper bound of $|V_i - V_{Th}|$. Thus, Eq. (2.12) becomes

$$\frac{\Delta P'}{\Delta P_{G_i}} \leq \frac{2\epsilon}{V_{min} - \epsilon}. \quad (2.13)$$

Suppose the voltage on the impedance Z_{Th} is V_Z , so $V_i = V_{Th} + V_Z$. Thus, $|V_i - V_{Th}|$ is maximized when $V_i = V_{max}$ and $V_{Th} = V_{min}$, as shown in Fig. 2.3, where θ is the phase angle of the impedance Z_{Th} . Thus, ϵ can be calculated as follows:

$$\epsilon = V_{max} \cos \theta - \sqrt{V_{min}^2 - V_{max}^2 + V_{max}^2 \cos^2 \theta}. \quad (2.14)$$

The impedance of transmission lines is usually much smaller than that of loads, so Z_{Th} is mainly determined by the impedance of a transmission line. In Z_{Th} , X_{Th} is usually 6-8 times smaller than R_{Th} (Laaksonen et al., 2005), so the phase angle θ is less than 10 degrees. Assuming V_{max} and V_{min} are equal to 1.1 and 0.9 of the normal voltage, respectively. Usually the voltage range is smaller, and then Eq. (2.13) is easier to satisfy. From Eq. (2.14), we get

$\epsilon \leq 0.185V_{\max}$. Based on this result, Eq. (2.13) becomes

$$\frac{\Delta P'}{\Delta P_{G_i}} \leq \frac{2 \times 0.185V_{\max}}{V_{\min} - 0.185V_{\max}} = 0.517. \quad (2.15)$$

The above result indicates that, when a PV system increases output power, the increment of power consumption is always smaller than the increased power. Considering all PV systems, the same result applies. As a result, PV systems can always increase output power to reduce P_0 until the reverse power flow exceeds the threshold or all PV systems reach the maximum output power. Since the proof is independent of the power sharing among PV systems, the above result is correct under our fairness definition. This means Lemma 1 is proved. \square

Lemma 2. If the voltage at any point $i \in \mathcal{N} \setminus \{0\}$ reaches its upper bound (i.e., $V_{\max} - \Delta_V^{ub}$), then no PV system can increase output power.

Proof. This lemma implies that, whenever a PV system increases its output power, voltages in all connecting points will exceed the upper bound. Thus, proving this lemma is equivalent to proving that $\frac{\partial |V_j|}{\partial P_{G_i}} > 0$ for all $i \in \mathcal{N}_1, j \in \mathcal{N} \setminus \{0\}$.

Considering i , we first prove that $\frac{\partial |V_i|}{\partial P_{G_i}} > 0$. On the Thevenin equivalent circuit in Fig. 2.2, suppose $V_{\text{Th}} = |V_{\text{Th}}| \angle 0$ is the reference voltage and S_1 is the power flowing to V_{Th} . Thus, $S_1 = (P_{G_i} - R_{\text{Th}}|I|^2) - jX_{\text{Th}}|I|^2$ and $V_i = V_{\text{Th}} + \frac{S_1^*}{V_{\text{Th}}} Z_{\text{Th}}$, where S_1^* is the complex conjugate of S_1 . As a result, the following equation is obtained:

$$V_i = V_{\text{Th}} + \frac{P_{G_i}R_{\text{Th}} - (R_{\text{Th}}^2 + X_{\text{Th}}^2)|I|^2}{V_{\text{Th}}} + j\frac{P_{G_i}X_{\text{Th}}}{V_{\text{Th}}}. \quad (2.16)$$

From this equation, we know that ΔV_i can be described as

$$\Delta V_i = \frac{R_{\text{Th}} \left(\Delta P_{G_i} - \left(1 + \frac{X_{\text{Th}}^2}{R_{\text{Th}}^2} \right) \Delta P' \right)}{V_{\text{Th}}} + j\frac{\Delta P_{G_i}X_{\text{Th}}}{V_{\text{Th}}}. \quad (2.17)$$

In Eq. (2.15), it is proved that $\Delta P' \leq 0.517\Delta P_{G_i}$. In addition, R_{Th} is 6-8 times larger than

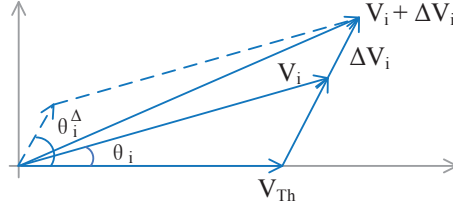


Figure 2.4: Phase relationship between V_i and ΔV_i

X_{Th} . Thus, the real part of ΔV_i is positive. Thus, the phase angle of ΔV_i is within $[0, \frac{\pi}{2}]$. From Eq. (2.16), V_i has a positive imaginary part. Moreover, $V_{Th}^2 \gg (R_{Th}^2 + X_{Th}^2) |I|^2$, so the real part of V_i is also positive. Thus, the phase angle of V_i is also within $[0, \frac{\pi}{2}]$. As a result, both V_i and ΔV_i are within the first quadrant, which implies that $|V_i + \Delta V_i| > |V_i|$ is always satisfied. Consequently, $\frac{\partial |V_i|}{\partial P_{G_i}} > 0$.

Next we prove that $\frac{\partial |V_j|}{\partial P_{G_i}} > 0$ for $j \neq i$. We know that $\frac{\partial |V_j|}{\partial P_{G_i}} > 0$ is equivalent to $|V_j + \Delta V_j| > |V_j|$. Moreover, if $|\theta_j - \theta_j^\Delta| < \frac{\pi}{2}$, where θ_j and θ_j^Δ are the phase angle of $|V_j|$ and $|V_j + \Delta V_j|$, respectively, then $|V_j + \Delta V_j| > |V_j|$. Thus, $|\theta_j - \theta_j^\Delta| < \frac{\pi}{2}$ provides a sufficient condition to ensure $\frac{\partial |V_j|}{\partial P_{G_i}} > 0$.

Define $\Theta = |\theta_j - \theta_i| + |\theta_i - \theta_i^\Delta| + |\theta_i^\Delta - \theta_j^\Delta|$. Since $|\theta_j - \theta_j^\Delta| \leq \Theta$, so if $\Theta < \frac{\pi}{2}$, then $|\theta_j - \theta_j^\Delta| < \frac{\pi}{2}$, which leads to $\frac{\partial |V_j|}{\partial P_i} > 0$. We evaluate three components of Θ as follows.

Firstly, $|\theta_i - \theta_i^\Delta|$ is studied. As analyzed in Eqs. (2.16) and (2.17), the relationship between V_{Th} , V_i and ΔV_i is illustrated in Fig. 2.4, which shows that $|\theta_i - \theta_i^\Delta| \leq \theta_i^\Delta$. Moreover, the phase angle is equal to

$$\theta_i^\Delta = \tan^{-1} \left(\frac{X_{Th}}{R_{Th}} \frac{\Delta P_{G_i}}{\Delta P_{G_i} - \left(1 + \frac{X_{Th}^2}{R_{Th}^2}\right) \Delta P'} \right) \quad (2.18)$$

where \tan^{-1} is the inverse tangent function. Since we know that $\frac{X_{Th}}{R_{Th}} < 1/6$ and $\Delta P'/\Delta P_{G_i} < 0.517$, so the θ_i^Δ is smaller than 20 degrees. Thus, $|\theta_i - \theta_i^\Delta|$ is also lower than 20 degrees.

Secondly, $|\theta_j - \theta_i|$ is studied. We use a Thevenin equivalent circuit to analyze the port between i and j . Since the impedance of loads is much larger than that of transmission lines, the equivalent impedance is mostly determined by the impedance of a transmission line, as shown in Fig. 2.5. In other words, the impedance of the Thevenin equivalent circuit in Fig. 2.5

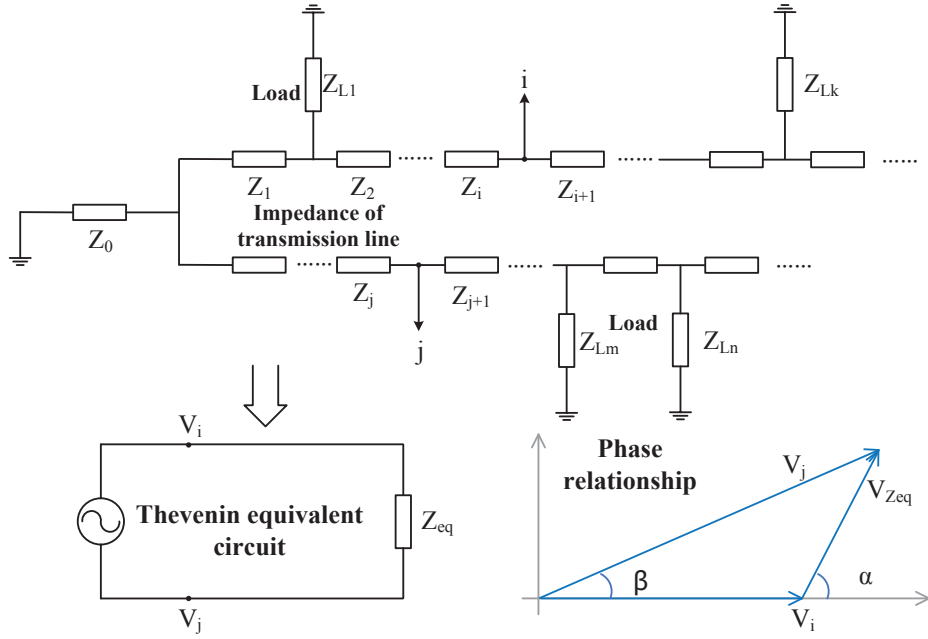


Figure 2.5: Thevenin equivalent circuit for the port between i and j

has the same phase angle as a transmission line. As shown in Fig. 2.5, the phase difference $\beta = |\theta_j - \theta_i|$ is smaller than the phase angle α of the transmission line. Since the phase angle of a transmission line is usually smaller than 10 degrees, so $|\theta_j - \theta_i|$ is lower than 10 degrees. Similarly, $|\theta_i^\Delta - \theta_j^\Delta|$ is smaller than 10 degrees.

As a result, $\Theta = |\theta_j - \theta_i| + |\theta_i - \theta_i^\Delta| + |\theta_i^\Delta - \theta_j^\Delta| < 40$ degrees. In other words, $|\theta_j - \theta_j^\Delta| < 40$ degrees, which implies that $\frac{\partial |V_j|}{\partial P_{G_i}} > 0$ for $j \neq i$. Consequently, we have shown that $\frac{\partial |V_j|}{\partial P_{G_i}} > 0$ for all $i \in \mathcal{N}_1, j \in \mathcal{N} \setminus \{0\}$, i.e., Lemma 2 is proved. \square

Theorem 2.1. *Maximum power allocation is achieved at all PV systems under any of the following three conditions: 1) Voltage upper bound is reached; 2) Reverse power flow reaches the threshold; 3) The maximum power points of all PV systems are reached.*

Proof. Considering condition 1), when any voltage reaches the upper bound, Lemma 1 shows that all PV systems have to stop increasing output power, i.e., maximum output power is achieved at all PV systems. From Lemma 1, when voltage upper bound is not reached, we can always increase output power of a PV system till condition 2) or 3) is satisfied. As a result,

optimal power points of PV systems are achieved under any of conditions 1), 2) and 3). \square

2.3 A Practical Distributed Scheme

The distributed scheme is implemented by three components, the central controller, PV systems and a wireless network. The design of the wireless network will be introduced in Section 2.4. In this section, the surplus allocation algorithm in the central controller and local power curtailment in PV systems are discussed in detail.

2.3.1 Surplus power allocation algorithm

Each PV system needs to report its surplus power $P_{S_i} = P_{G_i} - P_{L_i} \geq 0$ to the central controller. Assume there are n PV users. The total surplus power is then $\sum_{i=1}^n P_{S_i}$. The central controller can measure power flow from transformer P_0 and know the allowed reverse power P_0^{lb} , then the surplus power that can be allocated to PV systems is $P_S = P_0 - P_0^{lb} + \sum_{i=1}^n (P_{G_i} - P_{L_i})$. It is noticeable that P_S is actually the parameter c in Eq. (2.6). Combining with the k_i in Eq. (2.6), the new surplus power P_i allocated to PV system i can be calculated by Eq. (2.6). If P_i^{max} is unknown to the central controller, P_i^{max} is set to be infinite by default. The power point for PV system i is $P_{G_i} = P_i + P_{L_i}$.

2.3.2 Power curtailment in a PV system

In CPPT, power points are determined based on the status information reported from PV systems. However, due to network delay, loads of users may have changed before the distributed CPPT scheme finishes power tracking for all PV systems. If loads are dropped significantly, then the surplus power allocated to PV systems may result in over-voltage. Voltage curtailment is needed to respond to over-voltage. It is carried out by the inverter of a PV system. Once over-voltage is detected by the smart meter, the inverter immediately drops its power point to

track the local load (as measured by the smart meter). This approach can quickly stop power flow to the grid, and thus can effectively pull the voltage back to normal.

Effectiveness of Voltage Curtailment The following theorem states that voltage curtailment is effective.

Theorem 2.2. *The voltage curtailment scheme can resolve the over-voltage issue at all users (including those without PV systems) within one round of local power tracking.*

Proof. Over-voltage may occur in two cases.

Case 1: Over-voltage happens at user i , but voltages at its neighbors are normal. In this case, user i must have a PV system, because power flows from a higher voltage to a lower one. In response to over-voltage, the inverter for the PV system applies voltage curtailment by tracking the local load. After a delay of local power tracking, no active power will flow from user i to neighbors. Thus, the direction of power flow between users i and its neighbors is changed, and the voltage of user i must be lower than upstream neighbors and higher than downstream neighbors. Since these neighbors have a normal voltage level, the voltage at user i is now back to normal. As shown in Fig. 2.6, user 2 has a PV system and experiences over-voltage. After it has done voltage curtailment, the power will flow either from user 3 to 1 or the opposite, and thus user 2 has a normal voltage. This recovery process only takes the time of local power tracking, so it is completed within one round of power tracking.

Case 2: Over-voltage occurs at user i and also its neighbors, but other nearby users have normal voltage. If a user with no PV system has over-voltage, then some neighbors with the same over-voltage issue must have a PV system. Such neighbors with PV apply the voltage curtailment scheme, and then power flow is then changed. As shown in Fig. 2.6, users 6 and 8 have no PV but experience over-voltage, user 7 with a PV system has the same over-voltage issue, and other users have normal voltage. After the inverter of user 7 finishes local power tracking, power will flow either from user 5 to 9 or vice versa. No matter what direction of the

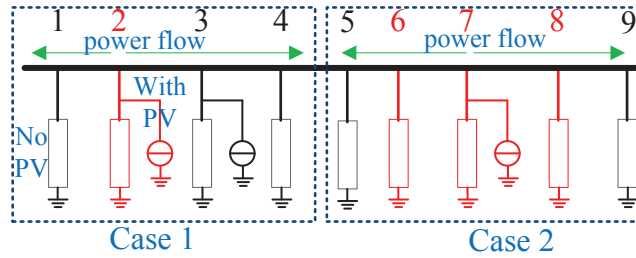


Figure 2.6: Illustration of two over-voltage cases

power flow, users 6, 7, or 8 recover their voltage to normal, since both user 5 and 9 have normal voltage. Thus, the over-voltage issue of case 2 can be resolved within one round of local power tracking. \square

2.3.3 Procedures of CPPT

The procedures of CPPT can be illustrated in Fig. 2.7. Msg_1 is sent by the central controller to announce allocated power point for PV systems. On reception of msg_1 , the inverters first track the power point contained in msg_1 and then respond the central controller with msg_2 . Msg_3 is periodically sent from inverters to the central controller to report their power points. Let T denote the periodic interval. At the beginning of every interval, inverters are required to send a msg_3 to the central controller. Once receiving these messages, the central controller decides if a new round of power allocation is needed. If a new round of power allocation is needed, the central controller sends msg_1 to inverters. Inverters respond with msg_2 once they receive msg_1 and finish local power tracking. In usual cases, the CPPT converges after several rounds of power allocation.

2.4 Network Design

CPPT is supported by a communication network between the central controller and inverters. Convergence of the distributed algorithm in CPPT depends on timely delivery of messages

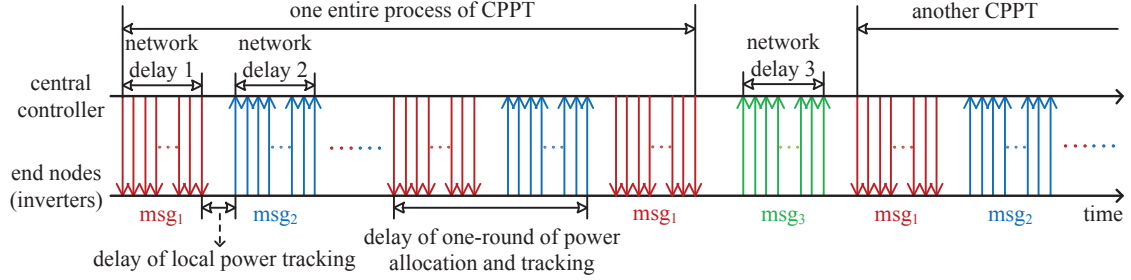


Figure 2.7: Timing relationship of messages between the central controller and inverters

between the central controller and all inverters. More specifically, the smaller the message delivery time is, the faster CPPT converges. Thus, the design goal of the communication network for CPPT is to minimize the message delivery time.

To achieve this goal, a communication network can be designed based on either wired or wireless network. Although optical networks are commonly deployed for distribution grid and substations, they are not readily available in distribution grid. Deploying a dedicated wired network (including power line communication network) for CPPT is a costly option. If public wired networks, such as the Internet connection, are used to carry traffic of CPPT, then it is necessary to request the service provider to guarantee QoS for CPPT, which is not an economical and feasible approach. As a result, wireless networks become a more viable option.

To cover an area (usually a few square kilometers or more) of a distribution grid, both cellular networks and wireless mesh networks (WMNs) can be adopted. However, we do not consider cellular networks in this paper for two reasons: 1) Frequent message exchange in CPPT results in high usage of cellular networks, which is too expensive; 2) A low rate cellular link results in high message delivery time, but a high rate cellular link is costly. Moreover, carrying CPPT messages through a cellular network has the same problem as that of a public wired network. Thus, the better choice for CPPT is WMN. In what follows, we focus on the design of a WMN such that proper operation of CPPT is ensured.

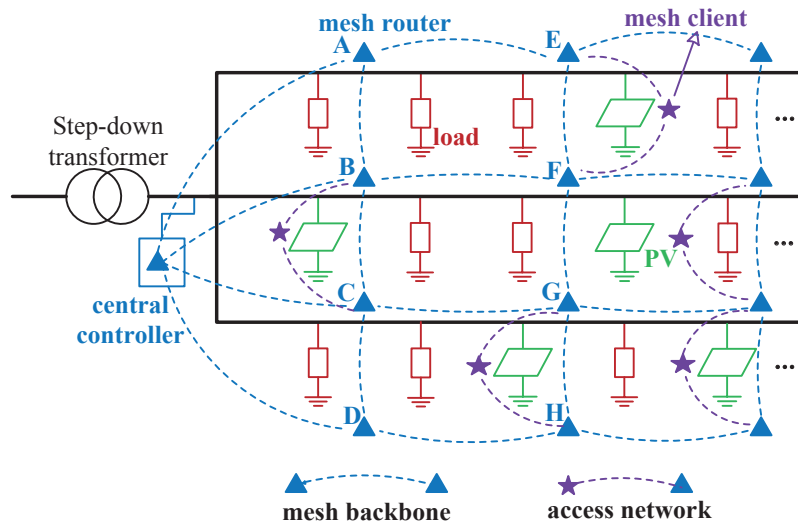


Figure 2.8: Two-layer hierarchical WMN for CPPT

2.4.1 Mesh Network Architecture for CPPT

Naturally the mesh network for CPPT consists of two hierarchy. The upper hierarchy consists of mesh routers that work in the same frequency channel and are connected like a multi-hop mesh network. It provides a wireless backbone to carry traffic between end nodes and the central controller. The lower hierarchy consists of access networks for end nodes (i.e., communication modules in inverters). A mesh router bridges an access network and the mesh backbone.

To avoid interference, the two hierarchies work in different frequency band, and neighboring access networks work in orthogonal frequency channels. In theory, one radio is sufficient to support all functions of a mesh router. However, to make protocol design simple, dual radio is considered, i.e., one radio for mesh backbone and the other for network access by end nodes.

Hierarchical Mesh Network Architecture The two-layer hierarchical WMN is depicted in Fig. 2.8, where the topology of a distribution sub-grid is also shown. The WMN takes reliability as a critical design factor. As a result, each branch of secondary feeders is covered by two different sets of mesh routers. As shown in Fig. 2.8, there are 4 sets of mesh routers deployed along three branches of the secondary feeders. As a result, the central controller is connected to 4 mesh routers, and each end node can be connected to two mesh routers.

WiFi Mesh versus Zigbee Mesh To build the hierarchical WMN for CPPT, there exist two major options: WiFi mesh or Zigbee mesh. In this paper, WiFi mesh is selected by considering the following factors:

- The communication nodes are not constrained by battery life, as they are co-located with power devices. Thus, Zigbee is not required.
- Considering a distribution sub-grid in a residential area, the communication distance between routers is usually in a range of about 100 meters. The distance between a mesh router and an end node is shorter than 100 meters. Thus, we do not need to rely on Zigbee to achieve long communication range.
- The raw data rate of Zigbee is only 20-250 Kbps, which is much lower than the 6 Mbps data rate of WiFi even if 1/2 BPSK is used. Since delay is critical to CPPT performance, so WiFi is a safer choice.

Although WiFi mesh is selected for CPPT, we do not conclude that Zigbee is infeasible for CPPT. How to make Zigbee work for CPPT is subject to future research. It should be noted that only a few end nodes are covered by a mesh router, so the new IEEE 802.11 protocol being developed for smart grid, i.e., IEEE 802.11ah, is not necessarily needed for CPPT.

2.4.2 Protocol Design

To ensure the CPPT algorithm converges fast and reliably, the communication delay in one round of CPPT must be minimized, subject to the constraint of link quality and network topology. To this end, we need to minimize the end-to-end delay of a message and also the number of messages involved in CPPT. To achieve this goal, a few design rules are followed:

- The timing relationship between different messages must be explored. In CPPT upstream messages and downstream messages are logically separated. Thus, message delivery pro-

protocols for downstream and upstream can be conducted separately for the benefit of a higher time efficiency.

- Different messages to the same destination need to be consolidated. The rationale behind this strategy is that the content of each message is small; fusing these messages can significantly reduce message delivery delay. For example, in the upstream, messages from different end nodes can be merged at their associated mesh router and then forwarded to the central controller through the mesh backbone.
- Protocols are designed specifically for the proper operation of CPPT. Thus, a complete protocol stack must be avoided. In fact, a protocol needs to be designed as simple as possible.

Considering the above design rules, we propose a *layer-2* message delivery protocol for CPPT. In this protocol, there is no transport or network layer; instead, CPPT messages are carried directly through a layer-2 protocol. Moreover, the layer-2 protocol runs separately for upstream and downstream messages.

Protocol for Downstream Messages Since each inverter needs to get a power point, message delivery from the central controller to all inverters is a one-to-many unicast problem. Unicast is required for reliable delivery, but one-to-many unicast results in large overhead and delay, if a conventional protocol stack like TCP/IP is followed. To avoid large delay and overhead, a layer-2 downstream protocol is design in this section.

With a layer-2 protocol, when a message is delivered to an end node, it needs to be carried hop-by-hop through the WMN till reaching the end node. However, a layer-2 routing is needed. Moreover, if all end nodes need to receive a message from the central controller, then the delay is high. To resolve these issues, two mechanisms are designed: i) power point information to all PV systems is consolidated in one message, and the central controller only needs to initiate one

message for all end nodes; ii) a directional flooding scheme is used in layer 2, so that the message from the central controller can be sent hop-by-hop to all mesh routers and their associated end nodes. Since reliability is critical, so the flooding actually conducts unicasting and requires ARQ. Thus, the directional flooding protocol is a *directional unicast flooding scheme*.

With the above ideas in mind, the downstream protocol works as follows:

1. Once the central controlled has determined power points for all PV systems, such information is consolidated into one downstream message, i.e., msg_1 .
2. The message is embedded into a layer-2 packet, and then sent to all neighboring mesh routers, e.g., A, B, C, D in Fig. 2.8, in a round-robin style. Once a mesh router, e.g., A , has received the message, it carries out two tasks. One is to flood the messages to all of its associated end nodes. The other is to forward the message to all of its neighboring routers except for the router that the message is received from. In this case, A forwards the message to B and E . However, when B receives the message, it discards it and knows that forwarding a message to A is not necessary.
3. Step ii) is repeated until all end nodes receive the message.

The layer-2 directional unicast flooding scheme is featured by several advantages: i) It matches the characteristics of downstream messages in CPPT; by nature delivering one message to all end nodes is a flooding process; ii) It eliminates transport layer reliability, and thus significantly reduces the end-to-end delay; iii) Routing is performed in layer 2 via a flooding process; iv) It is directional flooding, since a message always flows downstream to end nodes; v) Reliability is high, because flooding takes advantages of all links.

Protocol for Upstream Messages Similar to the downstream protocol, the upstream protocol is designed as a layer-2 protocol. However, since messages are initiated from different end nodes and then carried by the mesh backbone to the central controller, this process is much

different from a flooding process. Thus, a different layer-2 routing protocol is needed to forward a message all the way to the central controller.

The upstream protocol consists of three major mechanisms: i) message delivery from an end node to a mesh router ii) message fusion at mesh routers; iii) message forwarding through the mesh backbone to the central controller. The second mechanism is necessary to reduce traffic load from small messages, but it is simple; as a mesh router receives all messages of its associated end nodes, it consolidates these messages into one message. The details of the first and the third mechanisms are explained below.

Message delivery from an end node to a mesh router An end node can be associated with more than one mesh routers. All these mesh routers are considered as candidate routers to receive messages from the end node, but only one is selected based on a criterion such as the best link quality. The procedure of maintaining candidate mesh routers and selecting the best one is done in the background as part of the link management protocol. Once a mesh router is selected by an end node, it is informed of this selection via the link management protocol. Thus, a mesh router always knows how many end nodes are associated with it. Moreover, when a message (either msg_2 or msg_3) is initiated at an end node, it is sent to a specific mesh router.

There are two scenarios of upstream messages: msg_2 and msg_3 . For msg_2 , since it is initiated by an end node only upon the end of local power tracking, messages of msg_2 do not suffer from collisions due to concurrent transmissions. However, msg_3 is initiated periodically by end nodes. The proper operation of CPPT requires synchronization among end nodes. Thus, messages of msg_3 from different end nodes can easily collide due to concurrent transmissions at the beginning of each period. To avoid this issue, each end node starts a random backoff at the beginning of a period before sending msg_3 . This backoff is different from that in CSMA/CA. Usually CSMA/CA does not conduct backoff when a channel is clear and the backoff counter is zero.

Message forwarding in the mesh backbone A layer-2 routing protocol is designed to forward a message from a mesh router to the central controller. Similar to the first mechanism, each mesh router maintains a list of candidate mesh routers for message forwarding, but only one is selected for actual forwarding based on a criterion. Different from the first mechanism, two metrics are considered together as a criterion for selecting a mesh router: the link quality and the minimum hop to the central controller. Instead of choosing a mesh router with the best link quality, we select a mesh router that has a minimum-hop path to the central controller. However, the link quality along this path must be satisfactory; otherwise, the next candidate path is considered. Following the afore-mentioned process, each mesh router in the mesh backbone selects a mesh router as its next hop. As a result, once a message is received, it can be easily forwarded to the next hop till the central controller.

Our upstream layer-2 routing protocol are characterized by several features: i) *directional forwarding*, i.e., it selects the next-hop mesh router in the upstream to forward a message; ii) *multi-path routing*, because candidate routing paths are maintained; iii) *efficient forwarding*, i.e., messages are consolidated to reduce unnecessary overhead and delay. As a result, our layer-2 routing protocol is actually an efficient *directional multi-path layer-2 routing protocol*.

Impact of Link Quality To ensure reliability of message delivery, an erroneous message needs to be retransmitted. When link quality is low, multiple retransmissions are needed, which results in a large delay. The message delivery delay impacts the delay in reaction to the reverse power flow, as will be demonstrated in Section 2.5. When link quality degrades further, a node may lose all its available links to its neighbors. As a result, the connection between this node and the central controller is lost. However, such an event can be detected by both the node and the central controller. Based on the timing relations and message flows in Fig. 2.7, the central controller can find out that its association with an end node is lost either based on msg_2 or msg_3 . The central controller knows an end node is lost if it does not receive msg_2 from

the end node even after a timeout window expires. The length of the window is equal to the sum of the maximum network delays of msg_1 and msg_2 and the local tracking time. When the central controller does not receive msg_3 from an end node even after period T_p expires, it can also conclude that the end node is lost. Similarly, an end node knows it is isolated from the wireless network if it does not receive msg_1 from the central controller for a period longer than the sum of the maximum network delays of msg_1 and msg_3 .

After identifying an isolated end node, the central controller starts a new round of CPPT by excluding this node. For the isolated end node, it simply controls the output power of its PV system to track its local load. In this way, CPPT can still converge quickly after a few rounds, but the power points of PV systems are not optimal and fairness among PV systems is lost. However, since link failure is usually temporary, the time period in which fairness is impacted is negligible as compared to the power generation time of an entire day. In case a link failure is permanent, an isolated node can just simply turn off its PV and signal an alarm for network maintenance.

2.5 Performance Evaluation

To evaluate the performance of CPPT, several experiments are conducted through simulations on MATLAB platform. The physical system and the communication network are effectively integrated.

Physical System Setup A residential 220 V distribution sub-grid is considered with a 100 KVA transformer and 50 users. These users are connected to the transformer via 5 feeders with 10 users on each feeder. The impedance of these feeders is specified as in (Laaksonen et al., 2005). The distance between adjacent users is 40 m and the distance between transformer and the nearest user is 150 m. In the network, 50% random selected users are equipped with PV systems. One round of local power tracking time for a PV system is set to 0.01 s as in (Femia

et al., 2005). The areas of PV systems vary from 10 m^2 to 30 m^2 , and the efficiency of each PV system is set to 16.5%, i.e, a 10 m^2 PV system can generate 1.65 KW power if solar radiation is $1 \text{ KW}/\text{m}^2$. Hourly solar data in ([Online], 2008) is adopted to simulate the variation of solar radiation. In our experiments, each user has 12 types of appliances with an average power factor of 0.9. 20% of these appliances have rated power between 1 KW and 2 KW, while the rest consume power less than 1 KW. Load change of each user is modeled as a Poisson process with average frequency equal to 7 times/hour.

Communication Network Setup On both sides of the feeders, mesh routers are deployed uniformly so that each user can access at least 2 mesh routers. To mitigate interference, each mesh router is associated with at most 6 users. Moreover, 50 users are divided into 12 groups as in Fig. 2.9, where only half of the entire topology is illustrated. Users located in one green square belong to the same group and transmit their messages using the same channel on 2.4 GHz band. Adjacent groups adopt different channels. Also, the communications between mesh routers are conducted on a channel in 5.2 GHz band. The bandwidth of these channels are all equal to 20 MHz.

In addition, the size for each type of message is summarized as follow. msg_1 carries the power allocation information for 25 inverters, each with 6 bytes. This leads to a payload of 150 bytes. msg_2 and msg_3 are generated by inverters and include the system parameters. To carry such information, 15 bytes are required for a msg_2 or msg_3 from an inverter. After the message aggregation at a mesh router, the size of an aggregated msg_2 or msg_3 become 90 bytes at most, since there are at most 6 users associated with a mesh router.

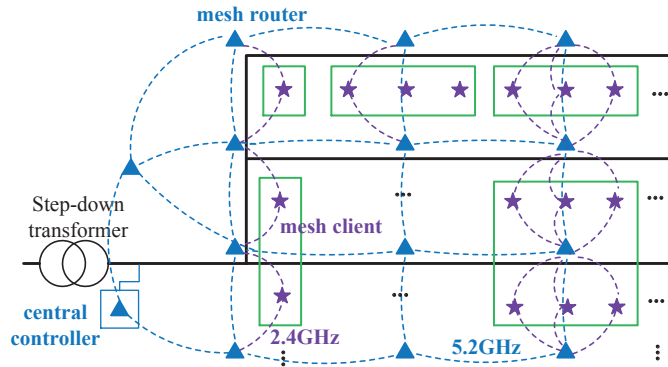


Figure 2.9: Communication network topology in experiments

2.5.1 Experiment Setup

2.5.2 Physical system evaluation

To investigate whether MPPT-based schemes can be effectively applied to distribution PV systems, the performance of MPPT and MPPT with voltage regulation (VR) is evaluated under our experiment setup. As shown in Fig. 2.10, performance results for three metrics are presented: the maximum voltage among all users (Fig. 2.10(a)), the reverse power flow at the transformer (Fig. 2.10(b)), and Jain fairness index of surplus power sharing (Fig. 2.10(c)). The formula for Jain index is $\mathcal{J} = (\sum_{i \in S} x_i)^2 / (n \sum_{i \in S} x_i^2)$, where S is the set of PV systems that are sending surplus power into grid, n is the number of PV systems in S , and $x_i = \frac{P_i}{k_i}$. From Fig. 2.10(a), it can be observed that the maximum user voltage always exceeds the safety threshold (i.e., V_{\max}) during day time, which is significantly detrimental to the distribution grid. This situation is alleviated when MPPT is combined with VR, which can effectively control user voltage to a reasonable value. However, MPPT with VR has other problems. As shown in Fig. 2.10(b), the reverse power at the transformer is higher than the maximum tolerable value (i.e., $P_0^b = -30$ KW). Moreover, the Jain index shown in Fig. 2.10(c) indicates that MPPT with VR incurs serious unfair share of surplus power between different users. The above results confirm that MPPT-based schemes are not effective to a distribution grid with PV cells.

To evaluate CPPT, a CPPT scheme denoted as CPPT30 (where “30” indicates the maximum

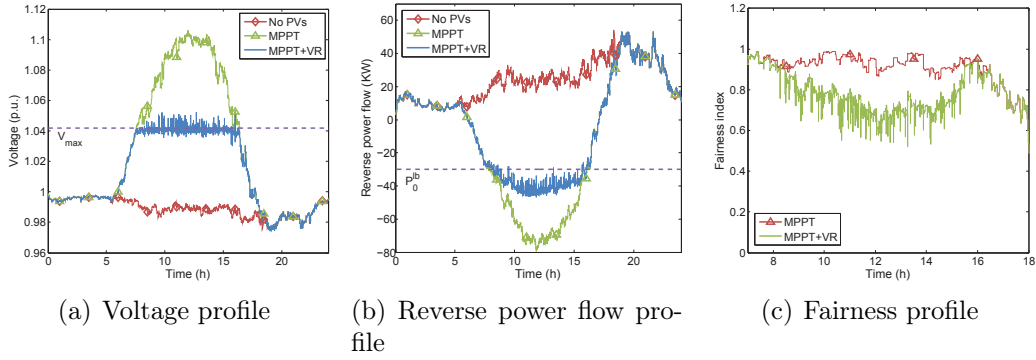


Figure 2.10: Performance of MPPT-based schemes.

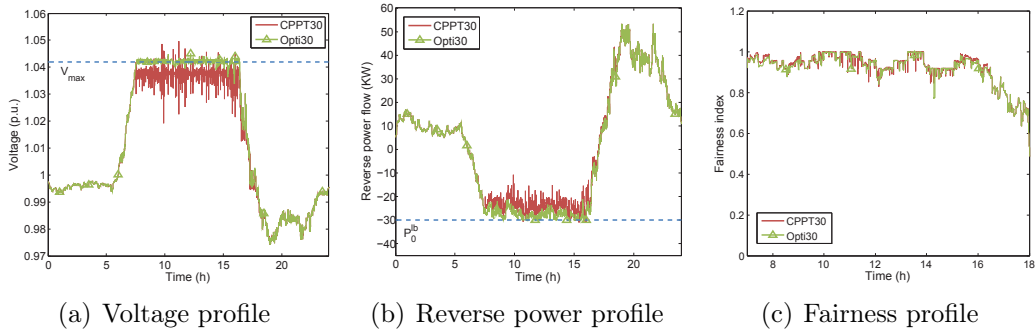


Figure 2.11: Performance of a CPPT scheme.

tolerable reverse power flow in KW) is considered first. In the experiments, the same setup as mentioned in Section 2.5.1 is adopted, and the average round-trip communication delay is 300 ms, which is a conservative value based on results shown in Section 2.5.4. This round-trip delay contains two parts. The first part is the downlink delay that is required to distribute messages from the central controller to all inverters. The second part is the waiting time of the central controller to collect all feedback messages from inverters. The power point tracking time is not included in this delay. For comparison, the performance for CPPT under ideal conditions, i.e., no communication and tracking delay, is also provided (denoted as Opti30). As shown in Fig. 2.11, the user voltage and the reverse power flow are well controlled with the CPPT scheme and the fairness index is significantly improved as compared to that of MPPT-based schemes. For all three performance metrics, the CPPT scheme closely follows the ideal CPPT (i.e., Opti30). The small gap is mainly due to the existence of the voltage margin ΔV^{ub} . All these results

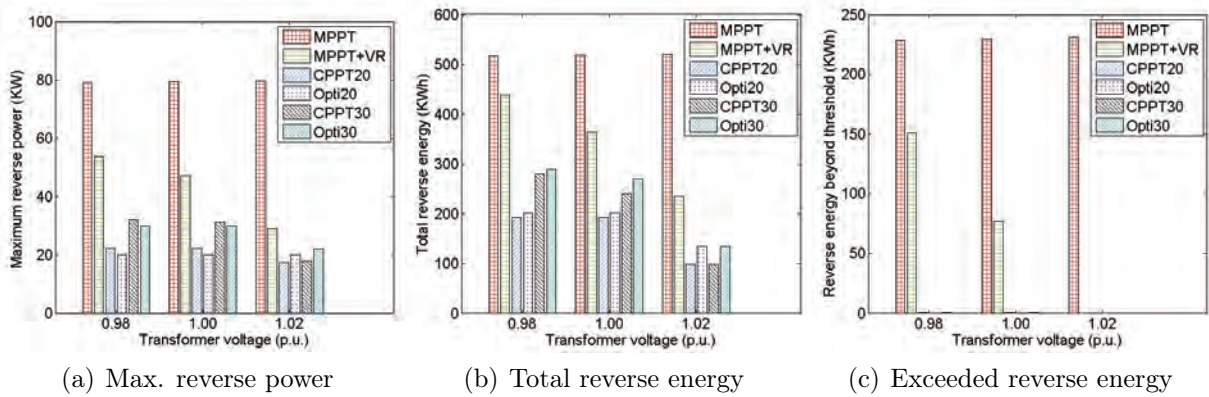


Figure 2.12: Performance of different schemes at different voltages

Table 2.1: Jain index under different transformer voltage levels

Voltage (p.u.)	Jain index			
	MPPT	MPPT+VR	CPPT30	Opti30
0.98	0.990	0.940	0.993	0.993
0.99	0.990	0.920	0.992	0.993
1.00	0.990	0.888	0.993	0.993
1.01	0.990	0.847	0.993	0.993
1.02	0.990	0.795	0.993	0.993
1.03	0.990	0.757	0.992	0.993

demonstrate the effectiveness of our CPPT scheme.

To further evaluate the performance of the CPPT scheme, we investigate three performance metrics under different voltage levels at the transformer. The results are shown in Fig. 2.12, Table 2.1, and Table 2.2, where the Jain index measures the fairness of surplus energy sharing among PV systems in a day, i.e., $x_i = \frac{E_i}{k_i}$ and E_i is the energy generated by PV system i . As the voltage level at the transformer increases, following results are observed: 1) the reverse power flow reduces; 2) the number of over-voltage occurrence increases; 3) the unfairness of MPPT with VR becomes more severe while that of CPPT remains unchanged. These results are attributed to the fact that users voltages increase as the voltage at the transformer rises. The voltage increase at user side suppresses the power injection from PV into the grid and also makes over-voltage occur more often. Since CPPT includes a mechanism of fine-grained coordination among different inverters, it effectively adapts voltage rise at the transformer,

Table 2.2: Over-voltage times and average rounds of CPPT in a day

Voltage (p.u.)	Over-voltage times		Average rounds for CPPT30
	MPPT+VR	CPPT30	
0.98	167	0	1.2
0.99	245	6	1.3
1.00	330	25	2.9
1.01	398	24	2.9
1.02	416	26	2.8

Table 2.3: Four parameters of the reverse power flow with respect to round-trip delay

Delay (ms)	Max. exceeded power (KW)		Exceeded energy (KWh)		Max. exceeded time (s)		Total exceeded time (s)	
	CPPT20	CPPT30	CPPT20	CPPT30	CPPT20	CPPT30	CPPT20	CPPT30
0	3.978	1.836	0.097	0.001	0.028	0.024	2.174	0.090
50	5.131	2.216	0.099	0.000	0.219	0.112	10.05	0.348
100	6.245	2.561	0.102	0.001	0.368	0.181	17.93	0.598
200	7.091	2.863	0.106	0.001	0.692	0.298	32.63	0.994
400	9.538	3.482	0.114	0.002	1.455	0.640	59.65	1.848
800	11.86	3.699	0.130	0.002	2.826	1.121	112.9	2.850

which shows a great advantage over the MPPT-based schemes. This experiment also shows an interesting result (see Table 2.2: the average rounds for CPPT to converge are within 3 times.

2.5.3 Relation Between Communication Delay and CPPT Performance

We conduct experiments to evaluate CPPT performance with respect to different round-trip delays. In these experiments, to capture abrupt and significant load variations, we consider an *extreme event* where 10 users with no PV systems pull out their own large appliances (1.5 KW) within 1 s. Thirteen such events are uniformly inserted into the period from 7 a.m. to 7 p.m. Also, Besides CPPT30 as mentioned previously, CPPT20 is also evaluated, where a more tight bound on the maximum reverse power flow, i.e. 20 KW, is imposed.

The variations of three metrics, i.e., times of over-voltage occurrence, Jain fairness index, and reverse power flow, under different round-trip delays are presented in Fig. 2.13, Table 2.3, and Table 2.4, respectively. From Fig. 2.13, it can be observed that the number of over-voltage occurrence in CPPT20 slowly increases with the communication delay and that of CPPT30

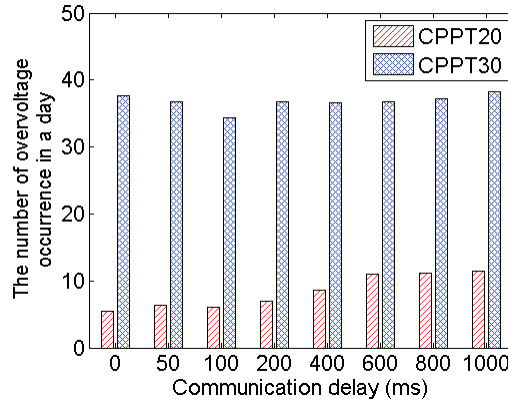


Figure 2.13: The number of over-voltage occurrence at different delays

Table 2.4: Fairness versus communication delay

Delay (ms)	Jain index	
	CPPT20	CPPT30
0	0.993	0.991
50	0.993	0.991
100	0.993	0.989
200	0.993	0.991
400	0.993	0.989
800	0.993	0.990

remains almost unchanged. Also, according to Table 2.4, the change of the Jain index in both CPPT20 and CPPT30 with respect to increasing communication delay is very small. This is because all inverters cooperatively adjust surplus power of their PV systems following the coordination of the central controller and hence the fairness is insensitive to the communication delay.

In contrast to Jain index and over-voltage occurrence, four parameters for the reverse power flow given in Table 2.3 are sensitive to the variations of the round-trip communication delay. The *exceeded power* indicates the power above the reverse power threshold. The *exceeded energy* indicates the total energy corresponding to the exceeded power. The *maximum exceeded time* is the maximum time period when the reverse power exceeds the threshold. The *total exceeded time* is the total time that the reverse power exceeds the threshold. As the round-trip delay increases, all these parameters increase apparently. In CPPT20, the reverse power may exceed

Table 2.5: Communication delay under different channel conditions

K	PER	QPSK		
		Uplink (ms)	Downlink (ms)	Round-trip (ms)
2	0.1767	34.6	34.3	68.9
3	0.0739	26.9	29.3	56.2
4	0.0143	23.3	28.2	51.5
6	0.0048	23.8	28.1	51.9
8	0	23.5	28.1	51.6
0	0.6	300	237	537

Table 2.6: Communication delay under different channel conditions

K	PER	BPSK		
		Uplink (ms)	Downlink (ms)	Round-trip (ms)
2	0.0096	30.7	55.0	85.7
3	0.0072	29.8	52.3	82.1
4	0	29.1	50.2	79.3
6	0	28.7	50.5	79.2
8	0	28.7	50.3	79.0

the threshold up to 12 KW, which severely violates the threshold and the total exceeded time is nearly doubled as the round-trip delay increases by twice. These results indicate that the reverse power flow is most significantly influenced by the round-trip delay, especially when the reverse power threshold is tighter (e.g. 20 KW in our simulation). Therefore, to control the reverse power flow properly, the round-trip delay must be reduced to a certain level.

2.5.4 Performance of the Communication Network

To determine whether the delay requirement imposed by the physical system can be achieved, several experiments are conducted to measure the round-trip delay under the network setting specified in Section 2.5.1. Since mesh routers and end nodes are intentionally installed in the line of sight for better link quality, Rician channel model is adopted to capture the fading effect in our simulation. To reflect different channel conditions, the K factor of Rician model varies from 2 to 8. The results for different transmission rates (corresponding to 1/2 BPSK and 1/2 QPSK) are shown in Table 2.5 and Table 2.6. It can be observed that the delay for 1/2 QPSK

is always smaller than that of 1/2 BPSK, which means a higher transmission rate is helpful to reduce the communication delay. However, the robustness of BPSK also neutralizes the negative effect of a lower transmission rate, and hence the delay difference between two cases is small. Actually, in all cases the round-trip delays for both BPSK and QPSK are basically controlled within 100 ms. By checking the results in Section 2.5.3, we know that such a WMN (with either modulation) is feasible for proper operation of CPPT.

We finally consider the case when link quality is extremely poor (due to significant out-of-network interference). As shown in Table 2.5 (labeled as $K = 0$), the packet error rate (PER) for QPSK can reach 60%. In this case, the round-trip delay degrades to 537 ms. According to the results in Section 2.5.3, this delay leads to a serious reverse power flow issue. This experiment shows the worst case scenario that definitely needs to be avoided. A possible solution to this problem is to develop a link recovery scheme based on cognitive radios. The detailed design is subject to future research. In case a link failure is permanent leading to missing messages, our CPPT scheme can still work properly.

2.6 Summary

In this chapter, a framework of coordinated power point tracking (CPPT) was developed for PV systems that are connected to a distribution grid. Under this framework, power points of all PV systems in the same distribution grid are controlled via a distributed and coordinated approach. Thus, issues such as over-voltage, reverse power flow, and fairness are all resolved while output power of PV systems is maximized. Wireless networks play a critical role in CPPT, so a hierarchical WMN was designed. More importantly, two layer-2 routing protocols were developed to support proper operation of CPPT. Simulation results demonstrated the advantages of CPPT over existing schemes. The effectiveness of the hierarchical WMN and the layer-2 routing protocols was also validated. The framework of CPPT gives us insights about

building other cyber-physical systems for smart grid. It also provides a systematic guideline for designing communication networks for a cyber-physical system.

Chapter 3

A Fair Queueing Scheme for Electric Vehicle Charging

3.1 Overall System Design

3.1.1 System Architecture

The typical architecture of a distribution grid is illustrated in Fig. 3.1, which consists of a medium voltage (MV) network where power is distributed to different distribution transformers and low voltage (LV) networks where power is consumed by users. In the MV network, voltage on the primary feeder is regulated by the on-load tap changer (OLTC) at substation and the switched capacitors or voltage regulators connected to the primary feeder. In the LV networks, there are switched capacitors aside by the secondary side of the distribution transformers to regulate the voltage on the secondary feeders. Before the incoming of EVs in high penetration levels, these devices in the MV and LV networks can control the voltage and power flow in their respective networks within operation ranges. In this way, the safety of the entire distribution grid can be ensured. These devices take control actions independently based on local measurements and no coordinations among devices are needed, which saves the cost of

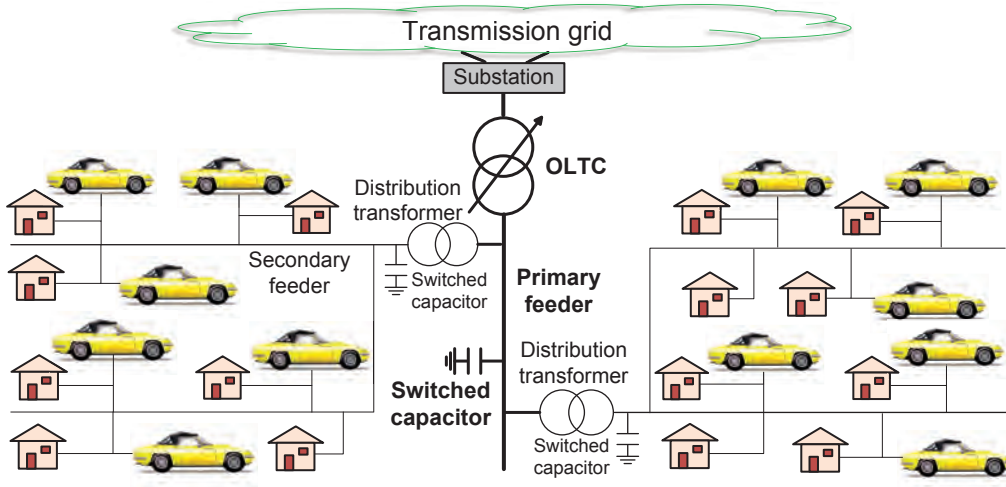


Figure 3.1: The major components in a sub-grid

communication infrastructures.

The incoming of EVs results in the overloading of the distribution transformers and the undervoltage problem at the secondary feeders. Therefore, the charging of EVs needs to be controlled. The simplest way to control EVs is to collect the data of all EVs to the substation and control the charging of EVs in a centralized way. However, the centralized control needs data collection and dissemination over a large area, which requires a costly communication infrastructure. To avoid this, the independence among the devices in the MV and LV networks needs to be utilized. To achieve this, users under different distribution transformers are controlled separately. The distribution transformer and its downstream users compose a *sub-grid*. In this way, the problem of controlling EVs in the entire distribution grid becomes the problem of controlling EVs in different sub-grids separately. The fairness among users under different sub-grids can be achieved by tuning the maximum allowable peak load in each sub-grid. For users in the same sub-grid, they locate in a much smaller area compared with the coverage of the entire distribution grid. Communication networking techniques can cover such areas with a low cost.

Fig. 3.2 shows the major components in a sub-grid. The voltage of users decreases along

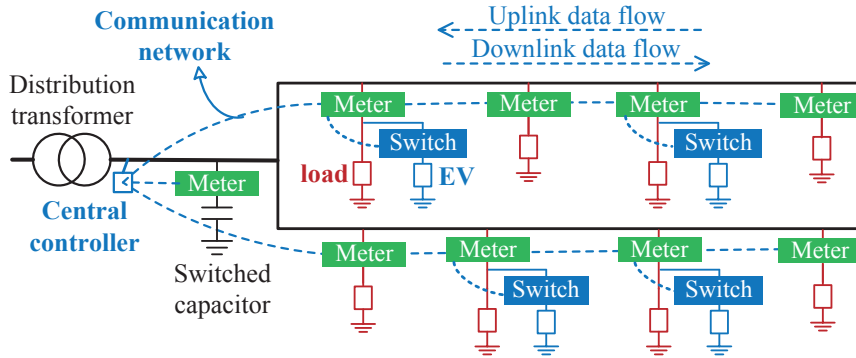


Figure 3.2: The major components in a sub-grid

the feeder. Users at the end of feeders have the lowest voltage that may become beyond the operation range. The smart meters are installed for users to detect the undervoltage problem immediately once it happens and informs the central controller of the problem via the communication network. Because topology of the sub-grid is usually unknown to the distribution grid operators, it is hard to identify which users are located at the end of feeders. Therefore, each user in the sub-grid is equipped with a smart meter. Further, the switched capacitor is equipped with a smart meter to monitor its injected reactive power and the central controller is equipped with a smart meter to measure the voltage and power flow at the connection point of the distribution transformer.

With these smart meters, real-time data of the sub-grid can be collected and the impedance matrix of the sub-grid can be easily calculated from the collected data*. Each EV is connected to the sub-grid with a switch that can control the on/off state of the EV and measure the power flow through it. The smart meter controls the states of EVs by the switch and obtains the power flow through the switch when the EV is turned on. The power flow through the switch is complex power. The magnitude of the complex power is considered as the power consumed by the EV, which is the apparent power with unit VA. In this way, the central controller can obtain the rated powers of the EVs being charged without communicating with EVs directly,

*Without inquiring the sufficient condition to calculate the impedance matrix of the sub-grid like in (Li et al., 2013), we assume the smart meters can measure voltage phasor and complex power flow at each connection point, so the impedance matrix can be easily calculated as in (Yang et al., 2010).

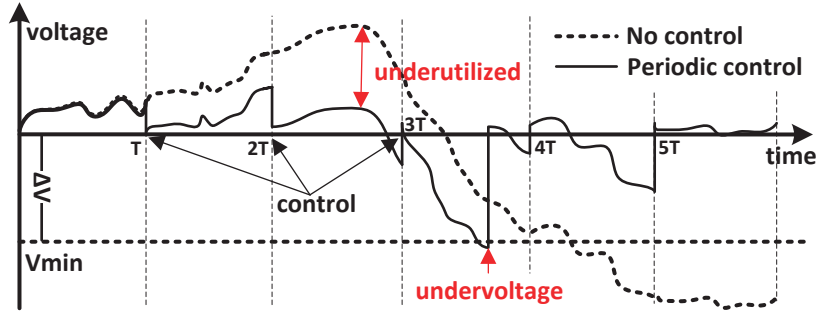


Figure 3.3: Voltage variations under periodic control and no control on EVs

no need to design a communication interface between EVs and the charging infrastructure. During the charging of an EV, the power of its charger is adaptive to the state of charge of the batteries. The switch can detect the change immediately and inform the central controller. Since there is no vehicle-to-grid technology available in this paper, the batteries of an EV can be regarded as a load. In the sub-grid, the only controllable loads are EVs. Other loads such as lights and air conditioners are taken as the basic loads of users, which cannot be controlled.

3.1.2 General Operations Inside a Sub-Grid

Periodic control and immediate undervoltage handling Since the distribution grid capacity is limited, we want to maximally utilize it to charge EVs. Whenever a user turns off a home appliance, there is a chance to charge one more EV. However, if control operations on EVs are conducted once there are load fluctuations, EVs will be frequently turned off/on, affecting the power quality. On the contrary, if control operations on EVs are not conducted for a long time, load fluctuations will be accumulated and result in the distribution grid capacity underutilized or the physical problems including undervoltage and transformer overloading. Therefore, we want to periodically control the states of EVs so that the distribution grid capacity can be better utilized and the probability of violating physical constraints can be reduced. Besides, periodic control provides a chance to switch the states of EVs so that the time lengths different EVs having been charged for can be adjusted, which maintains the fairness among EV users. It is not possible to completely avoid the physical problems, because even during a

short time period, the accumulated load fluctuations may become very large. Nonetheless, we can reduce the probability of violating the physical constraints to a low level by shortening the charging period.

Figure 3.3 shows the voltage variations under periodic control and no control on EVs, where the distribution grid is constrained by voltage. The states of EVs are controlled with a charging period, T . Control decisions on EVs are made at the beginning of each charging period. Unless overvoltage happens in the middle of a charging period, no other actions on EVs are made during a charging period. Once undervoltage happens, immediate actions should be taken to draw the voltage back to normal. The normal value is prescribed to be larger than $V_{\min} + \Delta V$, where V_{\min} is the lower bound of voltage operation range and ΔV is the safety margin. The safety margin is very important when the sub-grid operates at the margin of the voltage constraint, which makes the sub-grid resilient to load fluctuations. Let V_i be the voltage of user i and \mathcal{N} be the set of all users. The voltage of users should be controlled as

$$V_{\min} + \Delta V \leq V_i \leq V_{\max} - \Delta V, \quad \forall i \in \mathcal{N}, \quad (3.1)$$

where V^{\max} is the upper bound of voltage operation range. Let S_0 be the power flow through transformer, which is constrained as

$$|S_0| \leq S_0^{\max}, \quad (3.2)$$

where S_0^{\max} is the maximum allowable power flow through the transformer. There is no safety margin reserved for the power flow through transformer. The transformer overloading, whenever it happens, is solved at the beginning of the next charging period.

Generally, tolerable time for a violation of the physical constraints depends on its severity. According to IEEE Std C57.92, a distribution transformer can tolerate a loading three times the nameplate rating for less than half an hour in sacrifice of lifetime. The accumulated load fluctuations during a charging period are much smaller than the nameplate rating of transform-

ers and thus have merely no effects on the lifetime of transformers. Home appliances are very sensitive to undervoltage. A voltage sag to 70% of rated voltage for 0.5 s de-energizes some devices and an under-voltage to 80% of rated voltage for 0.5 s affects the performance of susceptible loads. When undervoltage happens, voltage is required to be drawn back to operation range within tolerable time so as not to affect the performance of loads which is prescribed in IEEE Standard 1250.

Control decisions on EVs and their implementations The control decisions on EVs in the beginning of a charging period prescribe the states of EVs in the charging period, which are made by the fair queueing scheme in Section 3.2. The decision-making process should take three problems into account: 1) the fairness among users 2) the safety of the sub-grid and 3) the power quality. The first two problems, as mentioned, are of significant importance, and we need more considerations on the third problem happening in implementing the control decisions. In consecutive charging periods, the states of EVs may be different. If we simply first turn off all EVs not in the charging period simultaneously and then turn on all EVs in the charging period, an abrupt voltage fluctuation will be induced, resulting in light flickers and affecting the power quality of users. We need more elaborately designed scheme to make and implement the control decisions. Besides, the process to implement control decisions takes some time in the beginning of each charging period. In a charging period, if no other events happen, the states of EVs will be first adjusted as prescribed by the control decisions and then the charging of EVs will proceed as controlled. However, events in the sub-grid may happen at any time. The disciplines to treat these events in a charging period need more discussions.

3.2 Fair Queueing for EV Charging

The generalized processor sharing (GPS) discipline can achieve perfect fairness for single-server queueing systems if queues can be served bit by bit. To approximate the performance of GPS,

many packetized queueing schemes are proposed to ensure each queue to get a fair share of resources. We want to utilize the properties of fair queueing to fairly allocate grid resources to EVs. When an EV is connected to the sub-grid, if it is not fully charged, the EV should be charged and considered as an active EV. To utilize the properties of fair queueing, the first step is to map the EV charging system in the sub-grid into a fair queueing system.

3.2.1 Mapping EV Charging System into a Queueing System

Multi-server queueing system with service preferences In the single-server queueing system, at any moment there is only one queue being served by the server. If each EV is regarded as a queue, due to the fact that several EVs can be charged in the sub-grid simultaneously, the sub-grid cannot be regarded as a single server, but a combination of many servers. Each server processes one packet from one queue at a time and packets from many queues can be served in parallel. A multi-server queueing system should be used for the mapping. In (Blanquer and Ozden, 2001), a multi-server queueing system is proposed. In the system, each queue can be served by each server, i.e., queues have no preferences towards servers. If packets can be served bit by bit, the multi-server system can be considered as a single-server GPS system, which is used as the reference system for the packetized model of the multi-server queueing system. However, in EV charging each EV only be charged by its own outlet, which means each EV has a preference towards servers and the preference is fixed. The multi-server system with queue preferences has been proposed in (Yap et al., 2013) as illustrated in Figure 3.4(a), where each queue can be served by several servers simultaneously. Our queueing system has simpler queue preferences, where each queue can only be served by one server as illustrated in Figure 3.4(b). The major difference between the two queueing systems is that in Figure 3.4(a), the output rates of servers depend only on channel conditions, while in our case, since the outlets are physically connected by transmission lines, the output rates of servers are coupled together and constrained by power grid constraints including voltage and power flow constraints.

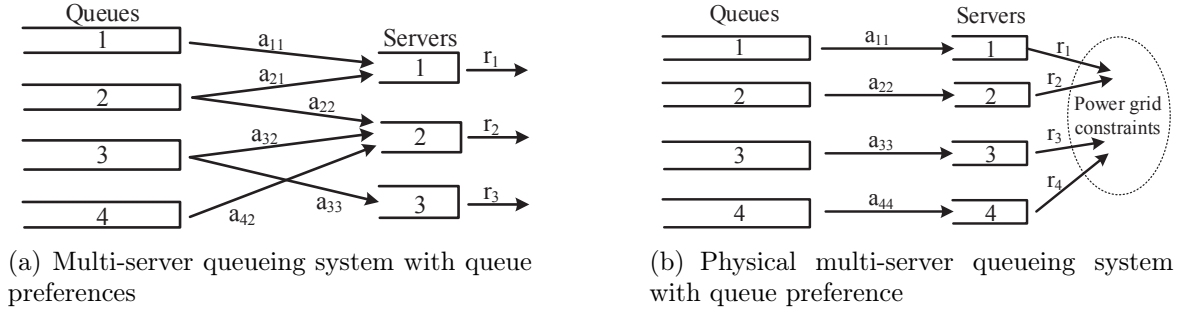


Figure 3.4: Illustration of the two multi-server queueing systems with queue preference

Energy packets in queues The states of EVs are controlled at the beginning of each charging period. An EV may be turned on in one charging period and turned off in the next charging period, which implies the required energy of EVs is charged in non-consecutive charging periods. The amount of energy each queue is served during a charging period is considered as an energy packet. Compared to the packets in information systems with packet length measured in bits, the lengths of energy packets are measured by joules. Unlike packets in information systems that arrive randomly, all the energy packets are backlogged into queues at the same time when the EV arrives. Because the required energy of EVs is unknown to the central controller, the central controller considers that every active queue has infinite packets backlogged in the queues. When an EV is fully charged or depart, it will stop charging. The central controller can detect that EV departs or is fully charged by monitoring the power flow through the outlet. Let \mathcal{Q} be the set of all active queues. Once EV i arrives, queue i is added into \mathcal{Q} . Let \bar{P}_i be the rated power of EV i and P_i be the service rate of server i .

Capacity of servers The capacity sum of servers is the power that the sub-grid uses to charge EVs, which is equal to the power flow through the distribution transformer minus the power consumed by user basic loads that cannot be controlled and the power loss on transmission lines. The capacity sum of servers reaches the maximum when the sub-grid capacity is used up, where the sub-grid capacity is defined as the maximum power that the sub-grid can provide. Due to the physical properties of the sub-grid, the sub-grid capacity depends on the locations

of loads being charged and the powers of the loads. For example, if the sub-grid capacity is constrained by voltage, i.e., undervoltage occurs first than transformer overloading, the sub-grid can support the charging of more EVs at the transformer's side than the charging of those at the end of secondary feeders. This is quite unlike the traditional queueing systems, where the capacity sum of servers is independent of the service rates of queues. Based on the above facts, we conclude that the capacity sum of servers can be determined only if a realization of EVs being charged is known first.

Weight of queues The weights of queues are determined before EVs start to be charged. EVs are expected to be charged the amount of energy proportional to their weights within the same charging time. However, in multi-server queueing systems with queue preferences, the service rates of queues are constrained by the capacity of servers. In the context of EV charging, the server rates of queues are further constrained by the rated power of EVs. How to allocate energy among EVs considering both their weights and the constraints of voltage, transformer capacity and the rated power of EVs will be discussed in Section 3.2.2.

The differences between events in information systems and sub-grid There exist two events in the sub-grid differing from those in information systems: 1) When undervoltage happens in the sub-grid, some EVs should be turned off immediately. The charging of EVs is interrupted while they are being charged. However, in information systems, when a packet is under transmission, the packet should be transmitted without preemption. 2) When a packet arrives in information systems, it can depart only when it finishes service, while in EV charging, EV can depart at any time. The event differences between the sub-grid and the information system result in some performance discrepancies. The queueing systems used in information system needs to be redesigned to handle the EV departures and the control parameters like the length of charging period should be adjusted to ensure the undervoltage happens with a very low probability. Only in this way, the performance provided by the queueing system is meaningful

for the EV charging.

3.2.2 Physical Multi-Server GPS (pMGPS)

In multi-server queueing systems with no queue preferences, if the queues can be served bit by bit, the service rates of queues under GPS discipline are proportional to their weights. However, with queue preferences, the services rate of queues are constrained by server rates. In (Yap et al., 2012), the definition of CPS is generalized to the case for multi-server GPS, where the service rates of queues follow a weighted max-min fair allocation at any moment. If EVs have continuous charging rates, we can utilize physical multi-server GPS to allocate power among EVs following the weighted max-min fairness. To do this, first assign the service rate of EV i to be zero, i.e., $P_i = 0$ and set Δx to be a very small number. In every iteration, increase the P_i by $w_i \Delta x$ for all $i \in \mathcal{Q}$ until one of the queues reach the following conditions: 1) P_i is close to the rated power of EV i , i.e., \bar{P}_i , less than $w_i \Delta x$. 2) P_i is close to the maximum power of the outlet less than Δx . 3) The minimum voltage in the sub-grid is close to the voltage lower bound or the power flow through the transformer is close to the transformer capacity. We now fix the rate of the EV and increase the rates of other EVs following the above procedures until all EVs have reached their rated power or the voltage and power flow are near the limits of operation range. In order to avoid undervoltage, the step size Δx needs to be small enough. We find that the above procedure to find the allocated power for EVs maximizes the EV with the minimum rated power first and then maximize other EVs, which is consistent with the definition of weighted max-min fairness.

Because the EVs only have on/off states, a queueing scheme that can schedule packets need to be designed. One of the most early work in fair queueing is the packet GPS (PGPS) (Parekh and Gallager, 1993) scheme, which uses the GPS as a reference system. By scheduling packets in the order they leave the referenced GPS system, the PGPS scheme can approximate the performance of GPS. If we use pMGPS as the reference and schedule packets in the order they

leave the pMGPS system, we will meet a problem incurred by the physical constraints of power grid. As mentioned the capacity sum of servers depend on the locations of EVs and the charging power of EVs. In pMGPS, EVs are charged with continuous powers, while in the packetized scheme, EVs are charged with rated power. The capacity sums of servers in the pMGPS and the packetized systems are different. In this case, the packetized scheme cannot approximate the performance of pMGPS. Therefore, we need to figure out other packetized schemes.

3.2.3 A Start-Time Fair Queueing Scheme for EV Charging

Because the output rates of servers are coupled, the multi-server deficit round robin in (Yap et al., 2013), where the servers operate separately, does not work. Even though we cannot use pMGPS directly as the reference system, we still want to have a reference system. As discussed, the reason why pMGPS cannot be used is because the capacity sum of servers in the packetized system is different from that in the pMGPS. To overcome this problem and utilize the reference system, we design a simulated multi-server GPS (sMGPS), which involves no physical processes like the pMGPS. The capacity sum of servers in the sMGPS system is always equal to that in the packetized system. The goal of the sMGPS is to simulate the weighted max-min fair allocation by using the capacity sum of servers from the packetized system. From the sMGPS, we can obtain the order that packets leave the sMGPS system, which in turn determines which packets are to selected in the packetized system.

The notion of virtual time has been used to schedule packets in many queueing schemes, of which WFQ (Parekh and Gallager, 1993), WF²Q (Bennett and Zhang, 1996) and self-clocked queueing (Golestani, 1994) uses the virtual finish times of packets for scheduling. The virtual finish times of packets reflect the order that packets finish service under the GPS discipline, which are calculated based on the weights of packets and the capacity sum of servers. In our case, the capacity sum of servers is not available and the virtual finish times of packets depend on future packet arrivals. Instead of using virtual finish times to schedule packets, start-time fair

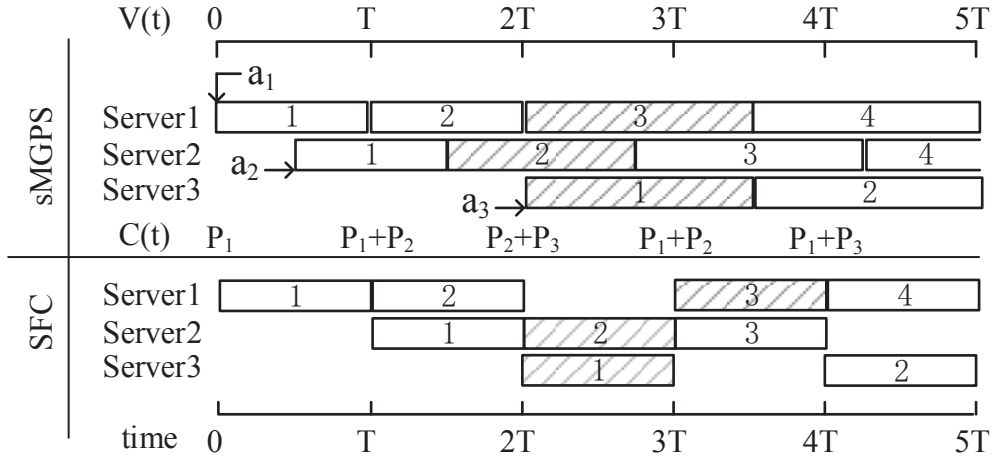


Figure 3.5: A toy example about how SFC works

queueing schemes propose to schedule packets based on their virtual start times. The virtual start times of energy segments can be obtained in our case, which can be used to provide an order for energy segments. With the order, we can obtain the capacity sum of servers. We call the start-time queueing system for EV charging as SFC system. In the SFC system, EVs with the smallest virtual start times are always selected first.

A toy example is used to illustrate how SFC works. There are three servers and three EVs of the same rated power in the sub-grid, but only two EVs can be charged in the sub-grid at any time. When time is zero, the virtual time of the sMGPS is also zero. At time zero, EV 1 arrives. The first packet of EV 1 is tagged with virtual time 0. The SFC system begins to select EVs based on their virtual start times. The first packet of EV 1 is selected and the selection process ends because no more EVs can be selected. During a charging period, there are no operations on the states of EVs. When EV 2 first arrives at time $\frac{T}{2}$, the first packet of EV 2 is tagged with virtual start time $\frac{T}{2}$. In the sMGPS system, the capacity sum of servers should fairly allocated to both EV 1 and 2. At time T , the virtual start times for the second packet of EV 1 and the first packet of EV 2 is T and $\frac{T}{2}$ respectively. Thus, EV 2 is first selected and then EV 1 is selected. The gray packets show the EV selections at time $3T$. When EV 3 arrives, the capacity sum of servers during $[2T, 3T]$ should be fairly allocated to three EVs.

Let $W_i^F(0, t)$ be the amount of energy EV i are charged in the F system during time $[0, t]$

and let $\mathcal{Q}^F(t)$ be the set of active queues in the F system at time t , where F can be the SFC, sMGPS and pMGPS systems. Let S_i^k be the virtual start time of the k -th packet in queue i . In information systems, when packets arrive, they will depart only when they finish service in the packetized system, which implies that $W_i^{\text{sMGPS}}(0, t) \leq W_i^{\text{SFC}}(0, t)$. However, in the EV charging system, EVs can depart at any time. If EV i depart at time t with $W_i^{\text{sMGPS}}(0, t) > W_i^{\text{SFC}}(0, t)$, which means the sMGPS system has allocated more energy to EV i than it needs. If the departure times of EVs are known in advance, the sMGPS will allocate this part of energy to other EVs in the system. Thus, we need to figure out a method to reallocate this part of energy back to the rest of EVs, where the method cannot interfere the order of packets sequence in the queueing system; otherwise, fairness cannot be guaranteed. The key idea of the method is to let the packets of EVs behave the same as those in the information systems, i.e., when queue i becomes empty in the packetized system, $W_i^{\text{sMGPS}}(0, t)$ must be less than $W_i^{\text{SFC}}(0, t)$. To achieve this, after queue i departs with $W_i^{\text{sMGPS}}(0, t) > W_i^{\text{SFC}}(0, t)$, we set the total length of packets backlogged in queue i as $W_i^{\text{sMGPS}}(0, t) - W_i^{\text{SFC}}(0, t)$, which means even when EV i departs, queue i is still nonempty. The packets in queues will be selected based on their virtual start times. However, when packets in queue i are selected, due to the departures of EVs, the physical impact of EV i on power grid does not exist. Therefore, EV i in this state is considered as a virtual EV, which has no physical impact on the power grid. With the method, after queue i becomes empty, the surplus energy allocated to queue i is reallocated to the rest EVs. The complete SFC scheme is as follows.

- Once EV i arrives at time t , all packets of EV i are backlogged into queue i in both the SFC and sMGPS systems. If queue i is in $\mathcal{Q}^{\text{SFC}}(t)$, EV i changes from virtual state to real; otherwise, queue i is added into both $\mathcal{Q}^{\text{sMGPS}}(t)$ and $\mathcal{Q}^{\text{SFC}}(t)$. Each packet p_i^k in the SFC system is tagged with the virtual time S_i^k when it begins service in the sMGPS system.
- At the beginning of each charging period, packets are selected for service in the increasing

order of their virtual start times until one of the following conditions is satisfied: 1) All the head-of-line packets with known virtual start times are selected. 2) Selecting one more EV will violate the physical constraints 3) All servers are serving a packet. 4) Selecting one more will make the total power of selected EVs in the SFC system larger than that of EVs with nonempty queues in the sMGPS system.

- When EV i departs or is fully charged at time t , if $W_i^{\text{sMGPS}}(0, t) > W_i^{\text{SFC}}(0, t)$, the total length of packets backlogged in queue i in the SFC system is set to be $W_i^{\text{sMGPS}}(0, t) - W_i^{\text{SFC}}(0, t)$ and EV i becomes virtual, which has no physical effects on power grid. Queue i is deleted from $\mathcal{Q}^{\text{sMGPS}}(t)$ when $W_i^{\text{sMGPS}}(0, t) = W_i^{\text{SFC}}(0, t)$. If $W_i^{\text{sMGPS}}(0, t) \leq W_i^{\text{SFC}}(0, t)$, the total length of packets backlogged in queue i in the sMGPS system is set to be $W_i^{\text{SFC}}(0, t) - W_i^{\text{sMGPS}}(0, t)$. Queue i is deleted from $\mathcal{Q}^{\text{sMGPS}}$ if all the packets in queue i finish service in the sMGPS system.
- When undervoltage happens, EVs are randomly chosen to be turned off so that the safety of power grid is ensured, but no change is made to the SFC and MGPS systems.

In the SFC system, the virtual finish times of packets are unable to predict. Let $n_i(t)$ and $m_i(t)$ be the number of packets that finish service in queue i until time t in queueing systems under SFC and GPS disciplines respectively and p_i^j be the j -th packet in queue i . The virtual start time of packet $p_i^{n_i(t)+1}$ is unknown, i.e., only the energy packets that start their service in the sMGPS system have determined virtual start times. The virtual start time of a packet in the SFC system is the virtual time when the packet starts its service in the sMGPS system. Based on the above rules, it seems that the SFC system works well, but we need to check if there exists a moment where no packets are of known virtual start times. If so, the SFC system has no EVs to select and thus cannot proceed. We will prove that under SFC, at least one EV in the sub-grid has known virtual start time.

Lemma 3. The SFC and sMGPS systems have the same busy periods and it suffices to bound the fairness measure for each busy period. In particular, for any time t ,

$$\sum_{i \in \mathcal{N}} W_i^{\text{SFC}}(0, t) = \sum_{i \in \mathcal{N}} W_i^{\text{sMGPS}}(0, t). \quad (3.3)$$

Proof. Let us consider the first busy period where the SFC and sMGPS systems both start at $t = 0$ and become idle at time t_1 and t_2 respectively. For any EV i that departs or is fully charged at time t' , if $W_i^{\text{sMGPS}}(0, t') > W_i^{\text{SFC}}(0, t')$, queue i in the SFC system becomes virtual and is deleted from $\mathcal{Q}^{\text{SFC}}(t')$ until backlogged packets are served at some time t^* , where $W_i^{\text{SFC}}(0, t^*) = W_i^{\text{sMGPS}}(0, t')$ and if $W_i^{\text{sMGPS}}(0, t') \leq W_i^{\text{SFC}}(0, t')$, the sMGPS system will continue to serve queue i until $W_i^{\text{sMGPS}}(0, t'') = W_i^{\text{SFC}}(0, t')$ at some time t'' and delete queue i from $\mathcal{Q}^{\text{sMGPS}}(t'')$. Thus, we have $W_i^{\text{sMGPS}}(0, t_1) = W_i^{\text{SFC}}(0, t_2)$ for all $i \in \mathcal{N}$, which implies $\sum_{i \in \mathcal{N}} W_i^{\text{SFC}}(0, t_1) = \sum_{i \in \mathcal{N}} W_i^{\text{sMGPS}}(0, t_2)$. In addition that the SFC and sMGPS systems have equal output rates, we can conclude $t_1 = t_2$. Because the SFC and sMGPS systems have the same output rate and the same busy periods, Eq. (3.3) follows. When the SFC and sMGPS systems are both idle at time t_1 , $W_i^{\text{sMGPS}}(0, t_1) = W_i^{\text{SFC}}(0, t_1), \forall i \in \mathcal{N}$. Therefore, the fairness measure can be bounded for each period. \square

Theorem 3.1. $S_i^{n_i(t)+1}$ cannot be unknown for all queue $i \in \mathcal{Q}^{\text{SFC}}(t)$ at any time t .

Proof. We prove the lemma by contradictions. If $S_i^{n_i(t)+1}$ is unknown for queue $i \in \mathcal{Q}^{\text{SFC}}(t)$, packet $p_i^{n_i(t)}$ must have not finished service in the sMGPS system, but it has finished service in the SFC system, which implies $W_i^{\text{sMGPS}}(0, t) < W_i^{\text{SFC}}(0, t)$. Assume $S_i^{n_i(t)+1}$ is unknown for all queue $i \in \mathcal{Q}^{\text{SFC}}(t)$ at some time t , then $\sum_{i \in \mathcal{Q}^{\text{SFC}}(t)} W_i^{\text{sMGPS}}(0, t) < \sum_{i \in \mathcal{Q}^{\text{SFC}}(t)} W_i^{\text{SFC}}(0, t)$. For queue $i \in \mathcal{Q}^{\text{sMGPS}}(t)$ but $i \notin \mathcal{Q}^{\text{SFC}}(t)$, queue i must satisfy $W_i^{\text{sMGPS}}(0, t) < W_i^{\text{SFC}}(0, t)$, because if $W_i^{\text{sMGPS}}(0, t) \geq W_i^{\text{SFC}}(0, t)$, there should be at least one packet in queue i the SFC system, i.e., queue $i \in \mathcal{Q}^{\text{SFC}}(t)$. For queue $i \notin \mathcal{Q}^{\text{sMGPS}}(t) \cup \mathcal{Q}^{\text{SFC}}(t)$, $W_i^{\text{sMGPS}}(0, t) = W_i^{\text{SFC}}(0, t)$. Therefore, we have $\sum_{i \in \mathcal{N}} W_i^{\text{GSPS}}(0, t) < \sum_{i \in \mathcal{N}} W_i^{\text{SFC}}(0, t)$, which contradicts Lemma 3. \square

However, even though we can prove there exists at least one EV, the sub-grid capacity cannot be fully utilized by only charging one EV. Thus, we need to develop an enhanced scheme, SFC+, on the top of the SFC. The SFC+ selects packets with known virtual start times the same as the SFC scheme. However, the SFC+ scheme also needs to select packets with unknown virtual start times. For queues whose head-of-line packet has unknown virtual start times, they are selected based on a metric. The metric, denoted as $\Delta_i(t)$, is calculated for each queue i , where $\Delta_i(t) = \frac{-FM_i(0,t)}{w_i \max_{i \in \mathcal{N}} \{\frac{L_i}{w_i}\}}$. The SFC+ always selects packets from queues with the smallest metric value first. The termination condition for the SFC+ is the same as that for the SFC.

3.3 Fairness Analysis of the SFC

The simulated GPS system is a reference. The difference between $W_i^{\text{sMGPS}}(0, t)$ and $W_i^{\text{SFC}}(0, t)$ indicates the performance gap between the SFC and sMGPS schemes for EV i . Denote the fairness measure $W_i^{\text{sMGPS}}(t_1, t_2) - W_i^{\text{SFC}}(t_1, t_2)$ for EV i during $[t_1, t_2]$ as $FM_i(t_1, t_2)$. We can conclude a scheme is fair if $FM_i(0, t)$ is a small constant for any $i \in \mathcal{N}$ and any time t .

Lemma 4. $FM_i(0, t)$ reaches the minimum when a packet in queue i finishes service in the SFC system and reaches the maximum when a packet in queue i begins service in the SFC system, which implies that $FM_i(0, t)$ reaches the maximum and minimum at the beginning of some charging periods.

Proof. In the SFC system, when queue i is in service, the slope of W_i^{SFC} is \hat{P}_i ; otherwise, the slope is 0. In the sMGPS system, the slope of W_i^{sMGPS} varies between 0 and \hat{P}_i . Thus, during a charging period if queue i is in service, $FM_i(0, t)$ is a non-increasing function with time; otherwise, $FM_i(0, t)$ is a non-decreasing function with time. $FM_i(0, t)$ reaches the minimum and maximum value at the end of a charging period when a packet in queue i in the SFC system finishes and begins service respectively. Because packets start and finish service only at the

beginning of charging periods, $FM_i(0, t)$ reaches the maximum and minimum at the beginning of some charging periods. \square

Lemma 5. For any queue i that is continuously backlogged during $[t_1, t_2]$,

$$\frac{W_i^{\text{sMGPS}}(t_1, t_2)}{W_j^{\text{sMGPS}}(t_1, t_2)} \leq \max\left(\frac{\hat{P}_i}{\hat{P}_j}, \frac{w_i}{w_j}\right). \quad (3.4)$$

Proof. If queue j is continuously backlogged during $[t_1, t_2]$,

$$\begin{aligned} \frac{W_i^{\text{sMGPS}}(t_1, t_2)}{W_j^{\text{sMGPS}}(t_1, t_2)} &\leq \frac{\int_{t_1}^{t_2} \min(r_i(t)C(t), \hat{P}_i) dt}{\int_{t_1}^{t_2} \min(r_j(t)C(t), \hat{P}_j) dt} \\ &\leq \frac{w_i \int_{t_1}^{t_2} \min(C(t), \hat{P}_i/w_i) dt}{w_j \int_{t_1}^{t_2} \min(C(t), \hat{P}_j/w_j) dt}, \end{aligned} \quad (3.5)$$

where $r_i(t)$ and $r_j(t)$ are the weight ratios of queues i and j over all queues in $\mathcal{Q}^{\text{sMGPS}}(t)$ respectively. If $\frac{\hat{P}_i}{w_i} > \frac{\hat{P}_j}{w_j}$,

$$\frac{W_i^{\text{sMGPS}}(t_1, t_2)}{W_j^{\text{sMGPS}}(t_1, t_2)} \leq \frac{w_i \frac{\hat{P}_i}{w_i} (t_1 - t_2)}{w_j \frac{\hat{P}_j}{w_j} (t_1 - t_2)} = \frac{\hat{P}_i}{\hat{P}_j};$$

otherwise,

$$\frac{W_i^{\text{sMGPS}}(t_1, t_2)}{W_j^{\text{sMGPS}}(t_1, t_2)} \leq \frac{w_i \int_{t_1}^{t_2} C(t) dt}{w_j \int_{t_1}^{t_2} C(t) dt} = \frac{w_i}{w_j}.$$

Thus, the lemma follows. \square

Theorem 3.2. For any time t and any queue i ,

$$-L_i \leq FM_i(0, t) \leq w_i \max_{i \in \mathcal{N}} \left\{ \frac{L_i}{w_i} \right\}. \quad (3.6)$$

Proof. We first prove the lower bound. Let t_1 be the time a packet in queue i in the SFC system finishes service. Then, we have $W_i^{\text{SFC}}(0, t_1) = n_i(t_1)L_i$. starts its service in the sMGPS

system, which implies $W_i^{\text{sMGPS}}(0, t_1) > (n_i(t_1) - 1)L_i$. Hence, $FM_i(0, t_1) \geq -L_i$.

Let t_2 be the time a packet in queue k begins service in the SFC system. At time t_2 , the $n_i(t_2)$ -th packet for all queue $i \in \mathcal{N}$ have finished service in the SFC system. Let t' be the time when the $n_i(t_2)$ -th packet for all queue $i \in \mathcal{N}$ have finished service in the sMGPS system. We show that $t' \geq t_2$. Assume that $t' < t_2$, which means $W_i^{\text{sMGPS}}(0, t') \geq W_i^{\text{SFC}}(0, t_2), \forall i \in \mathcal{N}$. Since $t' < t_2$, we have $W_i^{\text{sMGPS}}(0, t_2) > W_i^{\text{SFC}}(0, t_2), \forall i \in \mathcal{N}$, i.e., $\sum_{i \in \mathcal{N}} W_i^{\text{sMGPS}}(0, t_2) > \sum_{i \in \mathcal{N}} W_i^{\text{SFC}}(0, t_2)$, which contradicts Lemma 3, so $t' \geq t_2$.

Let p^* be the packet finishing service at t' and S^* be its virtual start time, where packet p^* is in queue i^* . Since p^* has started service before $p_k^{n_k(t_2)+1}$ in the SFC system, we have $S^* < S_k^{n_k(t_2)+1}$. Let t^* be the time packet p^* starts service in the sMGPS system. At time t^* , packet $p_k^{n_k(t_2)+1}$ has not started service in the sMGPS system, so $W_k^{\text{sMGPS}}(0, t^*) \leq n_k(t_2)L_k = W_k^{\text{SFC}}(0, t_2)$. Then,

$$\begin{aligned} FM_k(0, t) &\leq W_k^{\text{sMGPS}}(0, t') - W_k^{\text{sMGPS}}(0, t^*) \\ &\leq L_{i^*} \frac{W_k^{\text{sMGPS}}(t', t^*)}{W_{i^*}^{\text{sMGPS}}(t', t^*)}, \end{aligned} \quad (3.7)$$

Based on Lemma 5, if $\frac{\hat{P}_k}{\hat{P}_{i^*}} > \frac{w_k}{w_{i^*}}$,

$$FM_k(0, t) \leq L_{i^*} \frac{\hat{P}_k}{\hat{P}_{i^*}} = \hat{P}_k T = L_k; \quad (3.8)$$

otherwise,

$$FM_k(0, t) \leq L_{i^*} \frac{w_k}{w_{i^*}} = w_k \frac{L_{i^*}}{w_{i^*}} \leq w_k \max_{i \in \mathcal{N}} \left\{ \frac{L_i}{w_i} \right\}. \quad (3.9)$$

Therefore, $FM_k(0, t) \leq w_k \max_{i \in \mathcal{N}} \left\{ \frac{L_i}{w_i} \right\}$. \square

3.4 Fairness Analysis of the SFC+

Let $\mathcal{Q}_-^{\text{SFC}}(t)$ be the set of queues in $\mathcal{Q}^{\text{SFC}}(t)$ with fairness measure less than zero and let $\mathcal{Q}_+^{\text{SFC}}(t)$ be the set of queues in $\mathcal{Q}^{\text{SFC}}(t)$ but not in $\mathcal{Q}_-^{\text{SFC}}(t)$. Denote the number of queues in $\mathcal{Q}_+^{\text{SFC}}(t)$ and $\mathcal{Q}_-^{\text{SFC}}(t)$ as $|\mathcal{Q}_+^{\text{SFC}}(t)|$ and $|\mathcal{Q}_-^{\text{SFC}}(t)|$.

Lemma 6. For any time t ,

$$\sum_{i \in \mathcal{Q}_+^{\text{SFC}}(t)} FM_i(0, t) \leq \max_{i \in \mathcal{N}} \left\{ \frac{L_i}{w_i} \right\} \sum_{i \in \mathcal{Q}_+^{\text{SFC}}(t)} w_i, \quad (3.10)$$

Proof. Denote $\sum_{i \in \mathcal{Q}_+^{\text{SFC}}(t)} \hat{P}_i$ as $A(t)$. We prove the lemma in three cases. *Case 1:* $C(t) < A(t)$ for all time t . The SFC+ degenerates to the SFC. From Theorem 3.2, $FM_i(0, t) < w_i \max_{i \in \mathcal{N}} \left\{ \frac{L_i}{w_i} \right\}$ for all $i \in \mathcal{Q}_+^{\text{SFC}}(t)$, so the lemma follows trivially. *Case 2:* $C(t) \geq A(t)$ for all time t . Queues in $\mathcal{Q}_+^{\text{SFC}}(t)$ are always served. Let queue $i \in \mathcal{Q}_+^{\text{SFC}}(t)$ for $t \in [t_1, t_2]$. From Lemma 4, we have $FM_i(0, t_1) \geq FM_i(0, t_2)$. Thus, if $FM_i(0, t_1) \leq a_i$, we must have $FM_i(0, t) \leq a_i$ for any $t \in [t_1, t_2]$. Let t_1 be the time when $FM_i(0, t)$ becomes positive. There exists an integer m such that $t_1 \in [(m-1)T, mT]$ and $FM_i(0, (m-1)T) \leq 0$. From Lemma 4, we can conclude FM_i reaches the maximum at time mT . Since $FM_i(0, (m-1)T) \leq 0$, $FM_i(0, t_1) \leq FM_i(0, mT) \leq L_i$. The lemma follows.

Case 3: $C(t)$ is larger and less than $A(t)$ alternatively at different times. As the packets of queues begin service only at the beginning of charging periods, $C(t)$ varies at $t = mT$, where m is an integer. Let $[m_1T, m_2T)$ be the first time interval where $C(t) < A(t)$ and $[m_2T, m_3T)$ be the time interval where $C(t) \geq A(t)$. From Lemma 4, we know that for any queue i as long as $FM_i(0, m_2T) < a_i$, $FM_i(0, m_3T) < a_i$ for sure. Since $C(t) > A(t)$ for $t \in [0, m_1T)$, based on the conclusions in Case 2, $FM_i(0, m_1T) \leq L_i$ for queue $i \in \mathcal{Q}_+^{\text{SFC}}(m_1T)$. The lemma follows at time m_1T . We need to prove that the upper bound of $FM_i(t)$ for $t \in [m_1T, m_2T)$.

Case 3.1: There exists a queue k in $\mathcal{Q}_+^{\text{SFC}}(m_1T)$, but not in $\mathcal{Q}_+^{\text{SFC}}((m_1+1)T)$. Denote the

packet that begins service at time m_1T in queue k in the SFC system as p^* , the time p^* starts service in the sMGPS system as t^* and the time p^* finishes service in the sMPGS system as t' . Since queue $k \in \mathcal{Q}_-^{\text{SFC}}((m_1 + 1)T)$, the packet after p^* has not started service in sMGPS system at time $(m_1 + 1)T$, which implies $t' > (m_1 + 1)T$. As p^* begins service earlier than $p_i^{n_i((m_1+1)T)+1}$, we have

$$W_i^{\text{sMGPS}}(0, t') \leq n_i((m_1 + 1)T)L_i = W_i^{\text{SFC}}(0, (m_1 + 1)T).$$

Then, for any queue $i \in \mathcal{Q}_+^{\text{SFC}}((m_1 + 1)T)$,

$$FM_i((m_1 + 1)T) \leq W_i^{\text{sMPGS}}(0, t') - W_i^{\text{sMGPS}}(0, t^*).$$

Following Eq. (3.7)-(3.9), we can conclude that $FM_i(m_2T) \leq w_i \max_{i \in \mathcal{N}} \{\frac{L_i}{w_i}\}$. Hence, the lemma follows during $[m_1T, (m_1 + 1)T]$.

Case 3.2: There does not exist a queue k in $\mathcal{Q}_+^{\text{SFC}}(m_1T)$, but not in $\mathcal{Q}_+^{\text{SFC}}((m_1+1)T)$. Denote $\sum_{i \in \mathcal{Q}_+^{\text{SFC}}(t)} W_i^{\text{sMGPS}}(0, t)$ as $E_1(t)$ and $\sum_{i \in \mathcal{Q}_+^{\text{SFC}}(t)} W_i^{\text{SFC}}(0, t)$ as $E_2(t)$. Then, $E_2((m_1 + 1)T) = E_2(m_1T) + C(m_1T)T$. In the sMGPS system, the energy $C(m_1T)T$ is allocated to all active queues, which implies $E_1((m_1 + 1)T) < E_1(m_1T) + C(m_1T)T$. Thus,

$$\begin{aligned} E_1((m_1 + 1)T) - E_2((m_1 + 1)T) &< E_1(m_1T) - E_2(m_1T) \\ &= \sum_{i \in \mathcal{Q}_+^{\text{SFC}}(m_1T)} FM_i(m_1T) \leq \max_{i \in \mathcal{N}} \left\{ \frac{L_i}{w_i} \right\} \sum_{i \in \mathcal{Q}_+^{\text{SFC}}(m_1T)} w_i. \end{aligned}$$

Following the above cases, we can prove the lemma follows during $[(m_1 + 1)T, (m_1 + 2)T]$. Hence, the lemma follows during $[m_1T, m_2T]$, which implies that for any time t , $E_1(t) - E_2(t)$ is bounded as the lemma shows. \square

Theorem 3.3. *For any time t and any queue i ,*

$$FM_i(t) \leq L_i(\max_{i \in \mathcal{N}} \{ \frac{w_i}{L_i} \} \max_{i \in \mathcal{N}} \{ \frac{L_i}{w_i} \} + 1);$$

$$FM_i(t) \geq -(\max_{i \in \mathcal{N}} \{ \frac{w_i}{L_i} \} \max_{i \in \mathcal{N}} \{ \frac{L_i}{w_i} \} + 1) \sum_{i \in \mathcal{Q}_-^{sMGPS}(t)} L_i.$$

Proof. We first prove the upper bound. Let $m_i T$ be the time when $FM_i(t)$ reaches the maximum, denoted as M_i . From Lemma 6, we can see that $M_i < w_i \max_{i \in \mathcal{N}} \{ \frac{L_i}{w_i} \}$ for Case 1, 2 and 3.1. We need to bound $FM_i(t)$ for Case 3.1. Assume that $FM_i(0, m_i T) > M_i$. If queue i is selected at time $(m_i - 1)T$, from Lemma 4, we have $FM_i(0, (m_i - 1)T) \geq FM_i(0, m_i T)$. Thus, there should exist a time $m^* T < m_i T$ where queue i is not selected. Let $m^* T$ be the largest time before $m_i T$. We must have $FM_i(m_i^* T) > M_i - L_i$; otherwise, $FM_i(m_i T)$ cannot be larger than M_i . Since $p_i^{n_i(m^* T)+1}$ is not selected at time $m^* T$, other packets that are selected should have smaller virtual start times than $p_i^{n_i(m^* T)+1}$. Let t'_j be the time $p_j^{n_j(m^* T)+1}$ begins service in the sMGPS system for all $j \in \mathcal{Q}_+^{SFC}(m^* T)$. Then, $W_j^{sMGPS}(0, t'_j) = n_j(m^* T)L_j = W_j^{SFC}(0, m^* T)$ for all $j \in \mathcal{Q}_+^{SFC}(m^* T)$. From Lemma 5, we have

$$\begin{aligned} FM_j(0, m^* T) &= W_j^{sMGPS}(t'_j, m^* T) \geq W_j^{sMGPS}(t'_i, m^* T) \\ &\geq \frac{W_i^{sMGPS}(t'_i, m^* T)}{\max(\frac{\hat{P}_i}{\hat{P}_j}, \frac{w_i}{w_j})} \geq \frac{M_i - L_i}{\max(\frac{\hat{P}_i}{\hat{P}_j}, \frac{w_i}{w_j})} \end{aligned}$$

for all $j \in \mathcal{Q}_+^{SFC}(m^* T) \setminus \{i\}$, i.e., for all queues in $\mathcal{Q}_+^{SFC}(m^* T)$ except for queue i . Assume that

$$M_i - L_i > \max_{j \in \mathcal{Q}_+^{SFC}(m^* T)} \{ w_j \max_{i \in \mathcal{N}} \{ \frac{L_i}{w_i} \} \max(\frac{\hat{P}_i}{\hat{P}_j}, \frac{w_i}{w_j}) \}.$$

Then,

$$FM_j(0, m^* T) > w_j \max_{i \in \mathcal{N}} \{ \frac{L_i}{w_i} \}, \forall j \in \mathcal{Q}_+^{SFC}(m^* T),$$

which contradicts Lemma 6. Hence,

$$M_i - L_i \leq \max_{j \in \mathcal{N}} \{w_j \max_{i \in \mathcal{N}} \left\{ \frac{L_i}{w_i} \right\} \max\left(\frac{\hat{P}_i}{\hat{P}_j}, \frac{w_i}{w_j}\right)\}.$$

If $\frac{\hat{P}_i}{\hat{P}_j} < \frac{w_i}{w_j}$,

$$M_i - L_i \leq \hat{P}_i \max_{j \in \mathcal{N}} \left\{ \frac{w_i}{\hat{P}_i} \right\} \max_{i \in \mathcal{N}} \left\{ \frac{L_i}{w_i} \right\} \leq L_i \max_{j \in \mathcal{N}} \left\{ \frac{w_i}{L_i} \right\} \max_{i \in \mathcal{N}} \left\{ \frac{L_i}{w_i} \right\}; \quad (3.11)$$

otherwise,

$$M_i - L_i \leq w_i \max_{i \in \mathcal{N}} \left\{ \frac{L_i}{w_i} \right\} \leq L_i \frac{w_i}{L_i} \max_{i \in \mathcal{N}} \left\{ \frac{L_i}{w_i} \right\}. \quad (3.12)$$

Combining Eq. (3.11) and (3.12), we can conclude that

$$M_i \leq L_i \left(\max_{i \in \mathcal{N}} \left\{ \frac{w_i}{L_i} \right\} \max_{i \in \mathcal{N}} \left\{ \frac{L_i}{w_i} \right\} + 1 \right).$$

For the lower bound, as mentioned in (Parekh and Gallager, 1993; Blanquer and Ozden, 2001), if packets with unknown virtual start times are served, there does not exist a constant $c < 0$ such that $FM_i(0, t) > c$. The lower bound of $FM_i(0, t)$ depends on the number of queues in $\mathcal{Q}(t)$. Let queue $i \in \mathcal{Q}_-^{\text{SFC}}(t)$. Since $FM_j(t) < 0$ for queue $j \in \mathcal{Q}_-^{\text{SFC}}(t)$, based on Eq. (3.3), we have

$$FM_i(t) = - \sum_{j \in \mathcal{Q}_+^{\text{SFC}}(t) \setminus \{i\}} FM_j(t) \geq - \sum_{j \in \mathcal{Q}_-^{\text{sMGPS}}(t)} FM_j(t).$$

$FM_i(t)$ reaches the maximum when the upper bounds of all queues in $\mathcal{Q}_+^{\text{SFC}}(t)$ are reached and all queues in $\mathcal{Q}_-^{\text{SFC}}(t) \setminus \{i\}$ become empty simultaneously. This corresponds to the case when EVs in $\mathcal{Q}_-^{\text{sMGPS}}(t) \setminus \{i\}$ depart simultaneously. The lemma follows. \square

Lemma 7. For any time t ,

$$\sum_{i \in \mathcal{Q}_-^{\text{sMGPS}}(t)} FM_i(t) \geq - \max_{i \in \mathcal{N}} \left\{ \frac{L_i}{w_i} \right\} \sum_{i \in \mathcal{Q}_-^{\text{SFC}}(t)} w_i.$$

Proof. Because EVs may depart at any time t , $\mathcal{Q}^{\text{SFC}}(t)$ is not always equal to $\mathcal{Q}^{\text{sMGPS}}(t)$. Let queue $i \in \mathcal{Q}_+^{\text{SFC}}(t)$ for $t \in [t_1, t_2)$ and depart at time t_2 . According to the SFC scheme, queue i is in $\mathcal{Q}_+^{\text{sMGPS}}(t)$ during $[t_1, t_2)$. After time t_2 , queue i is deleted from $\mathcal{Q}_+^{\text{sMGPS}}(t)$, but queue i is still in $\mathcal{Q}_+^{\text{SFC}}(t)$ until all packets in queue i in the SFC system are served. Hence, if queue $i \in \mathcal{Q}_+^{\text{sMGPS}}(t)$, queue i must be in $\mathcal{Q}_+^{\text{SFC}}(t)$, i.e., $\mathcal{Q}_+^{\text{sMGPS}}(t) \subseteq \mathcal{Q}_+^{\text{SFC}}(t)$. Similarly, we can prove $\mathcal{Q}_-^{\text{SFC}}(t) \subseteq \mathcal{Q}_-^{\text{sMGPS}}(t)$. The set of queues that are nonempty in either the SFC or sMGPS system is equal to the union of $\mathcal{Q}^{\text{SFC}}(t)$ and $\mathcal{Q}^{\text{sMGPS}}(t)$, denoted as $\mathcal{Q}^{\text{SFC}}(t) \cup \mathcal{Q}^{\text{sMGPS}}(t)$. By the definition of $\mathcal{Q}^{\text{SFC}}(t)$ and $\mathcal{Q}^{\text{sMGPS}}(t)$, we have

$$\begin{aligned} & \mathcal{Q}^{\text{SFC}}(t) \cup \mathcal{Q}^{\text{sMGPS}}(t) \\ &= \mathcal{Q}_+^{\text{SFC}}(t) \cup \mathcal{Q}_-^{\text{SFC}}(t) \cup \mathcal{Q}_-^{\text{sMGPS}}(t) \cup \mathcal{Q}_+^{\text{sMGPS}}(t) \\ &= \mathcal{Q}_+^{\text{SFC}}(t) \cup \mathcal{Q}_-^{\text{sMGPS}}(t). \end{aligned} \quad (3.13)$$

For queue $i \notin \mathcal{Q}^{\text{SFC}}(t) \cup \mathcal{Q}^{\text{sMGPS}}(t)$, from Lemma 3, we have $FM_i(0, t) = 0$. Thus, Eq. (3.3) becomes,

$$\sum_{i \in \mathcal{Q}(t)} W_i^{\text{SFC}}(0, t) = \sum_{i \in \mathcal{Q}(t)} W_i^{\text{sMGPS}}(0, t),$$

where $\mathcal{Q}(t) = \mathcal{Q}_+^{\text{SFC}}(t) \cup \mathcal{Q}_-^{\text{sMGPS}}(t)$, which implies

$$\sum_{i \in \mathcal{Q}_+^{\text{SFC}}(t)} FM_i(t) + \sum_{i \in \mathcal{Q}_-^{\text{sMGPS}}(t)} FM_i(t) = 0. \quad (3.14)$$

The lemma follows from Lemma 6 and Eq. (3.14). \square

The lower bound in Lemma 3.3 can be achieved only when a large portion of EVs depart simultaneously. However, in real cases, EVs depart randomly. The number of EVs departing with fairness measure not equal to zero should be much smaller than the total number of EVs that are connected to the grid at any time. Then, the worst-case bound cannot well reflect the lower

bound of fairness measure in regular cases. We want to derive a bound for fairness measure in regular cases.

Theorem 3.4. *In regular cases,*

$$\mathbb{E}[FM_i(0, t)] > -([\log_2 |\mathcal{N}|] + 1)w_i \max_{i \in \mathcal{N}} \left\{ \frac{L_i}{w_i} \right\}. \quad (3.15)$$

Proof. Denote $\frac{-FM_i(0, t)}{w_i \max_{i \in \mathcal{N}} \left\{ \frac{L_i}{w_i} \right\}}$ as $\Delta_i(t)$. From Theorem 3.3, we know that for fixed number of EVs, $\Delta_i(t)$ is bounded for any $i \in \mathcal{N}$. For queue i_n , denote the time $\Delta_{i_n}(t)$ reaches the maximum as t_n and assume $\Delta_{i_n}(t_n) > n$. From Lemma 4, we know t_n is a multiple of charging periods. Because $\Delta_{i_n}(t_n)$ is the maximum, EV i_n must be selected at $t_n - T$; otherwise, $\Delta_{i_n}(0, t_n - T) \geq \Delta_{i_n}(0, t_n)$, where the equality holds when $W_i^{\text{sMGPS}}(t_n - T, t_n) = 0$, i.e., no EVs are selected at $t_n - T$. However, even if EV i_n is selected at $t_n - T$, we can still have $\Delta_{i_n}(0, t_n - T) = \Delta_{i_n}(0, t_n)$ if $W_{i_n}^{\text{sMGPS}}(t_n - T, t_n) = W_{i_n}^{\text{SFC}}(t_n - T, t_n) = P_{i_n}T$, which happens when all queues in $\mathcal{Q}^{\text{SFC}}(t_n - T)$ are selected. Since in regular cases EVs can be considered to depart with fairness measure equal to zero, $\mathcal{Q}^{\text{SFC}}(t)$ is always equal to $\mathcal{Q}^{\text{sMGPS}}(t_n - T)$. If all queues in $\mathcal{Q}^{\text{SFC}}(t_n - T)$ are selected, the slopes of $W_i^{\text{sMGPS}}(0, t)$ and $W_i^{\text{SFC}}(0, t)$ are both equal to \hat{P}_i during $[t_n - T, t_n]$ for any queue i , so $W_{i_n}^{\text{sMGPS}}(t_n - T, t_n) = W_{i_n}^{\text{SFC}}(t_n - T, t_n)$. In this case, $\Delta_{i_n}(t_n - T)$ is also the maximum. Let t_{n-1} be the largest time that is a multiple of T before time t_n such that $\Delta_{i_n}(0, t_{n-1}) < \Delta_{i_n}(0, t_n)$. Then, we have $W_{i_n}^{\text{SFC}}(t_{n-1}, t_n) - W_{i_n}^{\text{sMGPS}}(t_{n-1}, t_n) \leq L_i$. At time t_{n-1} , we have

$$\begin{aligned} \Delta_{i_n}(0, t_{n-1}) &= \Delta_{i_n}(0, t_n) - \Delta_{i_n}(t_{n-1}, t_n) \\ &= n - \frac{W_{i_n}^{\text{SFC}}(t_{n-1}, t_n) - W_{i_n}^{\text{sMGPS}}(t_{n-1}, t_n)}{w_i \max_{i \in \mathcal{N}} \left\{ \frac{L_i}{w_i} \right\}} \\ &\geq n - \frac{L_i}{w_i \max_{i \in \mathcal{N}} \left\{ \frac{L_i}{w_i} \right\}} \geq n - 1, \end{aligned}$$

where $w_i \max_{i \in \mathcal{N}} \left\{ \frac{L_i}{w_i} \right\} = L_i \frac{\max_{i \in \mathcal{N}} \{L_i/w_i\}}{L_i/w_i} \geq L_i$. At time t_{n-1} , not all queues are selected. For

queues with fairness measure less than zero, queues with the smallest Δ_i are selected first, which implies there exists at least one queue i_{n-1} with $\Delta_{i_{n-1}}(0, t_{n-1}) > (n-1)$. Similarly, for queue i_n , there exists time $t_{n-2} < t_{n-1}$ where $\Delta_{i_n}(0, t_{n-2}) > (n-2)$ and at least one queue i_{n-2} such that $\Delta_{i_{n-2}}(0, t_{n-2}) > (n-2)$; for queue i_{n-1} , there exists time $t_{n-3} < t_{n-1}$ where $\Delta_{i_{n-1}}(0, t_{n-3}) > (n-2)$ and at least one queue i_{n-3} such that $\Delta_{i_{n-3}}(0, t_{n-3}) > (n-2)$. Following this rule, we have

$$\Delta_{i_{n-j}}(0, t_{n-j}) > (n - (\lfloor \log_2 j \rfloor + 1)), \forall j = 1, \dots, r,$$

where $n - (\lfloor \log_2^r \rfloor + 1) = 1$, i.e., $r = 2^{n-1} - 1$. Next, we consider the value of $\Delta_{i_{n-j}}(0, t)$ at time $t = t_n$ for all $j = 0, \dots, r$. When $\Delta_{i_n}(0, t_{n-1})$ increases to $\Delta_{i_n}(0, t_n)$, $\Delta_{i_{n-1}}(0, t_{n-1})$ decreases to $\Delta_{i_{n-1}}(0, t_n) \geq (n-2)$. For queues i_{n-2} and i_{n-3} , when $\Delta_j(0, t_{n-2})$ increases to $\Delta_j(0, t_{n-1})$, $\Delta_j(0, t_{n-2})$ decreases to $\Delta_j(0, t_{n-1}) > (n-3)$ for $j = i_{n-2}, i_{n-3}$. However, from time t_{n-1} to t_n , queues i_{n-2} and i_{n-3} must be selected because $\Delta_j(0, t_{n-1}) < \Delta_{i_n}(0, t_{n-1})$ and thus $\Delta_j(0, t_n) > \Delta_j(0, t_{n-1}) > (k-3)$ for $j = i_{n-2}, i_{n-3}$. At time t_n , we have $\Delta_{i_n}(0, t_n) > n$ and

$$\Delta_{i_{n-j}}(0, t_n) > n - (\lfloor \log_2^j \rfloor + 2), \forall j = 1, \dots, r. \quad (3.16)$$

Then, we have

$$- \sum_{i=1}^r FM_i(0, t_n) \geq \max_{i \in \mathcal{N}} \left\{ \frac{L_i}{w_i} \right\} \sum_{j=0}^r w_{i_{n-j}} \Delta_{i_{n-j}}(0, t_n)$$

It follows from Eq. (3.16) and Lemma 7 that

$$\sum_{i \in \mathcal{Q}_-^{\text{SFC}^+}(t_n)} w_i \geq w_{i_n} n + \sum_{j=1}^r w_{i_{n-j}} (n - (\lfloor \log_2 j \rfloor + 2)) \quad (3.17)$$

Assume the weights of EVs are randomly selected by EV users, i.e., $\mathbb{E}[w_i] = c$ for all $i \in \mathcal{N}$,

where c is a constant. Then, by taking the expectation of both sides of Eq. (3.17), we have

$$|\mathcal{Q}^{\text{SFC}}(t_n)| \geq n + \sum_{j=1}^r n - (\lceil \log_2 j \rceil + 2) = 2^{n-1}$$

. Hence, $n \leq \log_2 |\mathcal{Q}^{\text{SFC}}(t_n)| + 1 < \lceil \log_2 |\mathcal{N}| \rceil + 1$. \square

Theorem 3.5. *For any time interval $[t_1, t_2] \gg T$, the total energy charged for EVs during $[t_1, t_2]$ under the SFC+ is no less than that in the pMGPS minus $\max_{i \in \mathcal{N}} \{\bar{P}_i\}(t_2 - t_1)$.*

Proof. We prove the Theorem in two cases.

Case 1: The power grid capacity is constrained by transformer capacity. Denote the energy EV i is charged during $[t_1, t_2]$ under the pMGPS as E_i . According to Gan et al. (2011), under the conditions that EV i should be charged E_i energy during $[t_1, t_2]$ and the charging powers of EVs are continuous, there exists a valley-filling charging profile that can minimize power loss. In other words, there exists a constant A such that

$$\sum_{i \in \mathcal{Q}(t)} P_i(t) = \min(A - D(t), \sum_{i \in \mathcal{Q}(t)} \bar{P}_i), \quad (3.18)$$

where $D(t)$ is the aggregated power of user loads. The theorem implies that as long as the charging profile is valley-filling, the power loss can be minimized, which is independent of how $A - D(t)$ is allocated among EVs. When transformer capacity is the active constraint of the sub-grid, A in Eq. (3.18) is equal to the transformer capacity. However, because the charging powers of EVs in SFC+ are not continuous, the transformer capacity cannot be used up. The SFC+ can only approximate the valley-filling charging profile. The maximum difference between the aggregated power under the pMGPS and SFC+ is $\max_{i \in \mathcal{N}} \{R_i\}$, which means the maximum difference between the total energy charged for EVs under pMGPS and SFC+ during $[t_1, t_2]$ is $\max_{i \in \mathcal{N}} \{R_i\}(t_2 - t_1)$. Next, we need to clarify how the SFC+ can charge E_i energy for EV i during $[t_1, t_2]$. The average power of EV i under pMGPS is $\frac{E_i}{t_2 - t_1}$. Let $f_i(t_1, t_2)$ be the time EV

can be charged during $[t_1, t_2]$. If $\frac{f_i(t_1, t_2)}{t_2 - t_1} = \frac{E_i}{(t_2 - t_1)P_i}$, the SFC+ fairly allocates energy the same as the pMGPS.

Case 2: The power grid capacity is constrained by voltage. Let α_{ij} be the voltage sensitivity of user i with respect to user j and $V_{i^*}(t)$ be the minimum voltage of all users at time t without EVs. After EVs are charged, the minimum voltage of all users becomes V_{\min} , where the minimum voltage usually happens at the end-of-line users. Since the locations of EVs are random and the charging powers of EVs in the pMGPS are distributed more evenly than those in the SFC+, the minimum voltage is still expected to happen at the end-of-line users. Let $\Delta V_{i^*}(t) = V_{i^*}(t) - V_{\min}$. Based on (Richardson et al., 2012), linearity between voltage and power of loads is an adequate approximation. Thus, we have

$$\begin{aligned} \Delta \bar{V}_{i^*} &= \frac{\int_{t_1}^{t_2} \Delta V_{i^*}(t) dt}{t_2 - t_1} = \sum_{j \in \mathcal{N}} \alpha_{i^*j} \int_{t_1}^{t_2} P_j(t) dt \\ &= \sum_{j \in \mathcal{N}} E_j \sum_{j \in \mathcal{N}} \alpha_{i^*j} \frac{\int_{t_1}^{t_2} P_j(t) dt}{\sum_{j \in \mathcal{N}} E_j} = \sum_{j \in \mathcal{N}} E_j \sum_{j \in \mathcal{N}} \alpha_{i^*j} \beta_j, \end{aligned} \quad (3.19)$$

where $\beta_j = \frac{\int_{t_1}^{t_2} P_j(t) dt}{\sum_{j \in \mathcal{N}} E_j}$.

In the SFC+, part of EVs are charged with full rates. The distribution of the power for EV charging is not even. Let $V_j(t)$ be the voltage of user j at time t , where $j \neq i^*$. Because the power for charging is not distributed evenly, even though $V_j(t) > V_{i^*}(t)$, $V_j(t)$ may become the minimum voltage in the sub-grid when EVs are charged. Let $\Delta V_j(t) = V_j(t) - V_{\min}$, so $\Delta V_j(t) > \Delta V_{i^*}(t)$. Following Eq. (3.19), we have

$$\Delta \bar{V}_j = \sum_{k \in \mathcal{N}} E'_k \sum_{k \in \mathcal{N}} \alpha_{jk} \beta'_k. \quad (3.20)$$

Because EVs locate randomly, for user j $\mathbb{E}[\alpha_{jk}] = \bar{a}_j$ and for user i^* , $\mathbb{E}[\alpha_{i^*j}] = a_{i^*}$. In addition that β_j and α_{i^*j} are independent, and $\sum_{i \in \mathcal{N}} \beta'_i = \sum_{i \in \mathcal{N}} \beta_i = 1$, we have $\sum_{k \in \mathcal{N}} E'_k = \frac{\mathbb{E}[\Delta \bar{V}_j]}{a_j}$

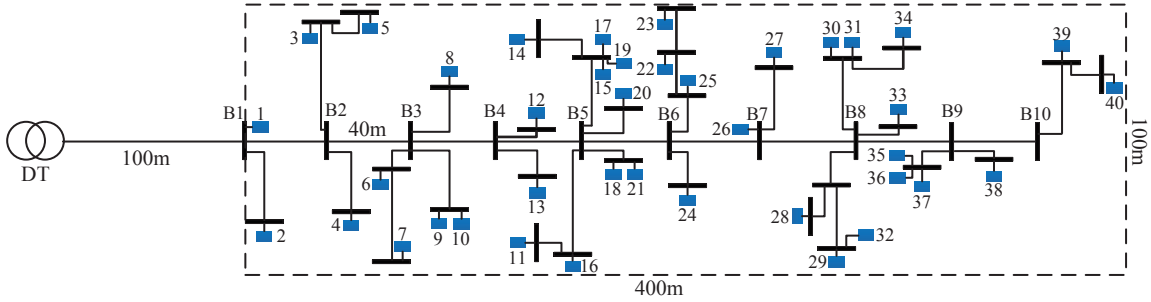


Figure 3.6: Physical topology of sub-grid used in experiments

and $\sum_{i \in \mathcal{N}} E_i = \frac{\mathbb{E}[\Delta \bar{V}_{i^*}]}{a_{i^*}}$. Thus, we can conclude that $\sum_{i \in \mathcal{N}} E'_i > \sum_{i \in \mathcal{N}} E_i$. \square

3.5 Performance Evaluation

To evaluate performance of the SFC and SFC+, we need to demonstrate that the bounds of fairness measure under the SFC and SFC+ are tight and the total energy charged for EVs under the SFC+ is close to that under the pMGPS. Experiments are conducted under typical user load profiles on MATLAB platform. The experiment setup and results are as follows.

3.5.1 Experimental Setup

The sub-grid is a single-phase 220 V network, which has a topology illustrated in Figure 3.6. There are totally 40 users randomly located in a 400m×100m rectangular area. The layout of transmission lines and buses is designed based on the locations of users, where the distances between adjacent buses from bus 1 to 10 are all equal to 40 m. A 100 kVA distribution transformer is 100 m away from bus 1. All transmission lines have the same impedance, which is $(0.375+j0.08)\Omega/\text{km}$. Each user has one EV with a random rated power x kW, $x \in \{2, 3, 4, 5, 6\}$ and battery size $4x$ kWh. The energy required by a user is randomly distributed from 40% to 100% of the battery size. The driving patterns of users are specified based on (Clement-Nyns et al., 2010). Besides the EV, each user has 15 types of appliances with an average power factor of 0.9, where 5 appliances have rated power between 1 kW and 2 kW and the rest have rated

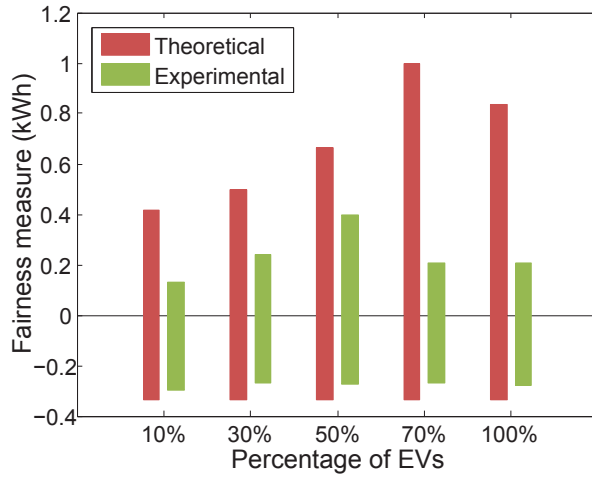


Figure 3.7: Worst-case bounds of fairness measure under the SFC

power less than 1 kW. The load change of each user is modelled as a Poisson process with an average frequency equal to 7 times/hour. All home appliances are prescribed to operate within voltage range from 0.92 to 1.042 p.u., where p.u. is the normalized voltage with respect to the base voltage 220 V. The safety margin of voltage is $\Delta V^{lb} = \Delta V^{ub} = 0.01$ p.u. The charging period is 5 minutes, i.e., $T = 5$.

3.5.2 Fairness performance of the SFC and SFC+

We have obtained the theoretical bounds of the SFC and SFC+. In this section, the theoretical bounds are verified by simulation results. As indicated by Lemma 3.2 and 3.3, the bounds of fairness measure among EVs differ. However, we can verify the bounds by checking if $\max_{i \in \mathcal{N}} \left\{ \frac{FM_i(0,t)}{w_i} \right\} \leq \max_{i \in \mathcal{N}} \left\{ \frac{L_i}{w_i} \right\}$ and $\max_{i \in \mathcal{N}} \left\{ \frac{FM_i(0,t)}{P_i} \right\} \geq -T$ for any time t . Figure 3.7 shows the theoretical and experimental bounds of fairness measure for the worst-case EVs under different penetration levels. The worst-case EVs have either the largest $\max_{i \in \mathcal{N}} \left\{ \frac{FM_i(0,t)}{w_i} \right\}$ or the smallest $\max_{i \in \mathcal{N}} \left\{ \frac{FM_i(0,t)}{P_i} \right\}$ for all time t . The theoretical bounds are close to the experimental bounds under different penetration levels.

Table 3.1 shows the theoretical and experimental bounds of fairness measure under the SFC+. Theoretical(R) represents for bounds under regular cases and theoretical(E) represents

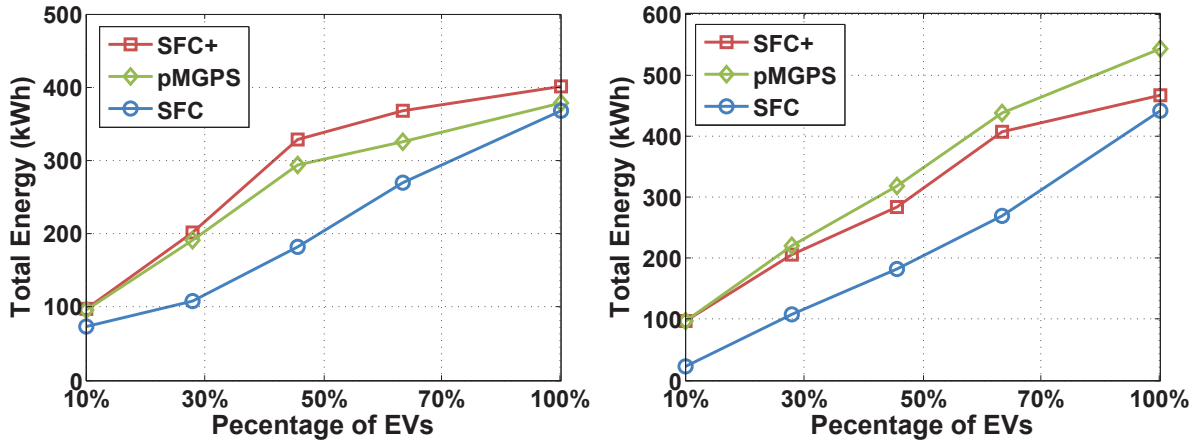
Table 3.1: Bounds of fairness measure under the SFC+

Percentage	Upper bound (kWh)		Lower bound (kWh)		
	Theoretical(E)	Experimental	Theoretical(E)	Theoretical(R)	Experimental
10%	2.00	0.06	-2.64	-5.0	-0.48
30%	1.83	0.39	-24.0	-8.3	-1.03
50%	3.00	0.40	-32.5	-10.0	-1.10
70%	4.33	0.46	-51.0	-10.0	-1.88
100%	3.67	0.49	-61.0	-11.7	-1.97

for bounds under extreme cases. From Table 3.1, we can see the experimental results are within the theoretical bounds. Even though the theoretical(R) is much tighter than theoretical(E), it is still much larger than the experimental bounds. Theoretical(E) describes the cases when a large portion of EVs depart simultaneously, which rarely happens. The theoretical(R) describes the cases when EVs depart randomly, but the theoretical(R) is independent of sub-grid capacity, which can be achieved only when the sub-grid capacity can be manipulated. However, in regular cases, the sub-grid capacity varies randomly, which results in the experimental bounds much smaller than the theoretical(R).

3.5.3 Total energy charged for EVs under the SFC+ and pMGPS

In both Figure 3.8(a) and 3.8(b), the SFC+ can achieve the total energy for EVs very close to the total energy under the pMGPS, which verifies the theoretical results in Lemma 3.5. Because under the SFC, only packets with known virtual start times can be selected, the SFC cannot fully utilize sub-grid capacity. The total energy for EVs under the SFC is much smaller than the total energy under the pMGPS and SFC+ under low penetration levels. However, as the penetration level increases, the total energy achieved by the SFC approaches to that under the SFC+ and pMGPS, because the total power of EVs that can be selected under SFC becomes larger than the sub-grid capacity. Therefore, when the penetration levels are high, the SFC can also fully utilize the sub-grid capacity. Since we have already verified the fairness performance



(a) Total energy charged for EVs when voltage is the active constraint (b) Total energy charged for EVs when transformer capacity is the active constraint

Figure 3.8: Total energy charged for EVs under the SFC, SFC+ and pMGPS schemes when sub-grid capacity is constrained by voltage and transformer capacity respectively.

of the SFC+, we can conclude that the SFC+ can achieve as good performance as the pMGPS.

3.6 Summary

In this chapter, a framework was developed to coordinate the charging of EVs connected to a distribution grid in a centralized way. The goal of the coordination is to fairly and efficiently allocate the distribution grid capacity to charge EVs under the constraints of voltage range and transformer capacity. To achieve this goal, two fair queueing schemes, SFC and SFC+, were designed to decide on/off states of EVs. The SFC scheme was proved to have only one packet difference from the referenced multi-server GPS system but the efficiency of utilizing power grid capacity is low. The SFC+ overcomes the disadvantages of SFC and was proved to achieve as good performance as the ideal physical multi-server GPS. The framework for EV charging can be extended to design other cyber-physical systems in smart grid. Further, emerging communication techniques can be easily incorporated into the framework for smart grid applications.

Chapter 4

Conclusion

Compared to the applications of communication technologies for daily and industrial use, the number of communication technologies in power grid is still very limited. To leverage the advantages of communication technologies, we need to figure out the requirements of power grid on wireless communications and develop a systematic guideline for communication network design for smart grid. Two smart grid applications, i.e., the integration of PVs and EVs, were studied in this thesis. In both applications, the safety of the distribution grid was ensured by communication networks. Without the support of communication networks, the power grid can either have a poor performance or be damaged due to the violations of physical constraints including voltage and transformer capacity. A complete framework was developed for the integration of PVs and EVs. The framework included the entire procedures about designing a system for integrating PVs and EVs into power grid, which can be easily extended to other cyber-physical systems in smart grid. Besides the demonstration of the dependence between the distribution grid and communication networks, a distributed power tracking algorithm for PV systems and new fair queueing schemes for EV charging were developed. The performance of the algorithm and the fair queue schemes was rigorously proved and verified by extensive simulations.

We have published our results for PV systems in a top journal in communication areas and a regular conference. More specifically, the two papers are (Wang et al., 2014) and (Pi et al., 2013), while the work on EVs is prepared to be submitted to the IEEE Transactions on Smart Grid.

4.1 Contributions

Compared to the related work, our work has the following contributions:

- A complete framework for integrating PV systems into power grid is developed. From the overall system architecture to the detailed designs, the framework includes complete procedures about how to design a system for PV systems. The framework can be easily extended to design other CPSs for smart grid.
- An optimization problem for power allocation among PV systems is formulated and the condition for optimal solution is obtained. The optimal condition requires no information on the topology of the distribution grid, which eliminates the limitations of the state-of-the-art schemes.
- A distributed power point tracking scheme is designed following a weighted max-min fair share algorithm. Based on this scheme and the conditions of the optimal power points, a practical and distributed procedure is developed for CPPT. Abnormal voltage or reverse power flow is also properly handled by the procedure.
- A wireless mesh network (WMN) is designed to ensure the proper operation of CPPT. The performance of the WMN is validated through extensive simulations.
- A complete framework for EV charging in the distribution grid is developed. The framework quantitatively shows the requirements of power grid on wireless networks, which

demonstrates the tightly-coupled relation between the distribution grid and wireless network.

- A physical multi-server GPS is proposed to achieve perfect max-min fairness. However, the physical multi-server GPS is not directly applicable. Two packetized fair queueing schemes, SFC and SFC+, are proposed based on the simulated MGPS.
- The fairness performance of the SFC and SFC+ is rigorously proved. The SFC can achieve nearly perfect fairness at the sacrifice of power grid capacity, while the SFC+ can fully utilize power grid capacity with satisfied fairness performance. Moreover, the SFC+ is proved to have as good performance as the pMGPS.

4.2 Future Work

Besides the work on the integration of PVs and EVs, I also find some very interesting research topics on the new emerging standard 802.11ah. The IEEE 802.11ah is an amendment of the IEEE 802.11. Compared with the 802.11, 802.11ah can support a large scale of sensor nodes and a long listen interval, which is suitable for smart grid communications. In smart grid, sensor nodes have been widely used such as the power line monitoring, water and gas meters at home and etc. Because these sensors are usually installed in places where no power is available, one of the most important research topics for sensors is to extend their lifetime. Over the years, many approaches have been proposed to help sensor nodes save energy. However, different from the mechanisms discussed in many approaches, 802.11ah AP periodically sends beacons to manage the network. Non-AP nodes can sleep for several days and wake up to receive a packet from AP. AP informs non-AP nodes of the packet by containing the packet information in beacons. For non-AP nodes, they have to receive specific beacons to decide if there is a packet for them. After a sleep time for several days, the clock drift between non-AP nodes and AP is large. Receiving the specific beacons with minimum energy is a challenging problem.

The above characteristics of 802.11ah make it unique from other protocols. Both the receiver-initiated and sender-initiated approaches can not be used, because waking up periodically is energy-consuming. I plan to design a new MAC protocol for power saving in 802.11ah as future work.

Acknowledgments

I would like to express my gratitude to all who have give me help during my master study.

First, I want to thank my advisor, Prof. Xudong Wang. He has paid great efforts and time in supervising me. Under his instruction, I have gradually become an experienced researcher during the past three years. He has helped me cultivate the habits of critical thinking and taught me how to conduct innovative research. He showed great patience when I made mistakes and always encouraged me to do better.

Second, I am grateful to my committee members, Prof. Jun Zhang, Xinen Zhu and Chien-Pin Chen. They have given me great suggestions to my presentation. Also, I want to thank my group members, Wenguang Mao, Shanshan Wu, Pengfei Huang, Aimin Tang, Yuhang Zhang, Chao Xu and Lingyang Ma for their accompaniment and help.

At last, I want to give my sincere gratitude to my parents for their support. They always respect my own choice and support me selflessly.

Appendix A

Publications

- **Y. Pi** and X. Wang, “A fair queueing scheme for electric vehicle charging,” *To be submitted to the IEEE Transactions on Smart Grid*.
- X. Wang, **Y. Pi**, W. Mao, and H. Qian, “Network coordinated power point tracking for grid-connected photovoltaic systems,” *IEEE Journal on Selected Areas in Communications*, 2014.
- **Y. Pi**, Y. Zhang, X. Wang, and H. Qian, “A cyber-physical framework towards smart grid wireless communications,” In *Proceedings of the 2013 International Conference on ICT Convergence (ICTC)*.

Bibliography

- Anand, S., B. G. Fernandes, and M. Guerrero (2013). Distributed control to ensure proportional load sharing and improve voltage regulation in low-voltage DC microgrids. *IEEE Transactions on Power Electronics* 28(4), 1900–1913.
- Ardakanian, O., C. Rosenberg, , and S. Keshav (2013). Distributed control of electric vehicle charging. In *Proceedings of the fourth international conference on future energy systems*, pp. 101–102.
- Balducci, P. J. (2008). Plug-in hybrid electric vehicle market penetration scenarios. Pacific Northwest National Laboratory.
- Bennett, J. C. and H. Zhang (1996). WF²Q: Worst-case fair weighted fair queueing. pp. 120–128.
- Blanquer, J. M. and B. Ozden (2001). Fair queueing for aggregated multiple links. In *Proceedings of the 2001 SIGCOMM conference, SIGCOMM'01*. ACM.
- Cipcigan, L. M. and P. C. Taylor (2007). Investigation of the reverse power flow requirements of high penetrations of small-scale embedded generation. *IET Renewable Power Generation* 1(3), 160–166.
- Clement-Nyns, K., E. Haesen, and J. Driesen (2010). The impact of charging plug-in hybrid electric vehicles on a residential distribution grid. *IEEE Transactions on Power Systems* 25(1), 371–380.
- DallAnese, E., H. Zhu, and G. B. Giannakis (2013). Distributed optimal power flow for smart microgrids. *IEEE Transactions on Smart Grid* 4(3), 1464–1475.
- Deilami, S., A. S. Masoum, P. S. Moses, and M. A. Masoum (2011). Real-time coordination of plug-in electric vehicle charging in smart grids to minimize power losses and improve voltage profile. *IEEE Transactions on Smart Grid* 2(3), 456–467.

- Esrām, T. and P. L. Chapman (2007). Comparison of photovoltaic array maximum power point tracking techniques. *IEEE Transaction on Energy Conversion* 22(2), 439–449.
- Esrām, T. and P. L. Chapman (2009). Clustered PV inverters in LV networks: An overview of impacts and comparison of voltage control strategies. In *Electrical Power and Energy Conference (EPEC), 2009 IEEE*, pp. 1–6. IEEE.
- Femia, N., G. S. G. Petrone, and M. Vitelli (2005). Optimization of perturb and observe maximum power point tracking method. *IEEE Transactions on Power Electronics* 20(4), 963–973.
- Gan, L., U. Topcu, and S. Low (2011). Optimal decentralized protocols for electric vehicle charging. In *IEEE Conference on Decision and Control (CDC)*. IEEE.
- Golestani, S. J. (1994). A self-clocked fair queueing scheme for broadband applications. 2, 636.
- Green, M. A., K. Emery, Y. Hishikawa, W. Warta, and E. D. Dunlop (2012). Solar cell efficiency tables (version 40). *Progress in photovoltaics: research and applications* 20(1), 12–20.
- Laaksonen, H., P. Saari, and R. Komulainen (2005). Voltage and frequency control of inverter based weak LV network microgrid. In *2005 International Conference on Future Power Systems*. IEEE.
- Lam, A., B. Zhang, and D. N. Tse (2012). Distributed algorithms for optimal power flow problem. In *2012 IEEE 51st Annual Conference on Decision and Control*. IEEE.
- Lavaei, J. and S. H. Low (2010). Convexification of optimal power flow problem. In *2010 48th Annual Allerton Conference on Communication, Control, and Computing (Allerton)*. IEEE.
- [Online] (2008). http://rredc.nrel.gov/solar/old_data/nsrdb/.
- Li, X., H. V. Poor, and A. Scaglione (2013). Blind topology identification for power systems. In *2013 IEEE International Conference on Smart Grid Communications (SmartGridComm)*. IEEE.
- Liew, S. N. and G. Strbac (2002). Maximising penetration of wind generation in existing distribution networks. In *IEE Proceedings of Generation Transmission Distribution*, pp. 256 – 262. IEE.

- Parekh, K. A. and R. G. Gallager (1993). A generalized processor sharing approach to flow control in integrated services networks: The single-node case. *1*(3), 344 – 357.
- Pi, Y., Y. Zhang, X. Wang, and H. Huang (2013). A cyber-physical system framework for smart grid wireless communications. In *2013 International Conference on ICT Convergence (ICTC)*. IEEE.
- Richardson, P., D. Flynn, and A. Keane (2012). Optimal charging of electric vehicles in low-voltage distribution systems. *IEEE Transactions on Power Systems* *27*(1), 268–279.
- Short, T. A. (2004). *Electric Power Distribution Handbook*. CRC press.
- Song, D., J. Xiong, Z. Hu, G. Li, and et al (2012). Progress in n-type Si solar cell and module technology for high efficiency and low cost. In *2012 38th IEEE Photovoltaic Specialists Conference (PVSC)*, Volume 20, pp. 3004–3008. IEEE.
- Sortomme, E., M. M. MacPherson, and S. S. Venkata (2011). Coordinated charging of plug-in hybrid electric vehicles to minimize distribution system losses. *IEEE Transactions on Smart Grid* *2*(1), 198–205.
- Sundstrom, O. and C. Binding (2012). Flexible charging optimization for electric vehicles considering distribution grid constraints. *IEEE Transactions on Smart Grid* *1*(3), 26–37.
- Tonkoski, R., L. A. C. Lopes, and T. H. M. El-Fouly (2011). Coordinated active power curtailment of grid connected PV inverters for overvoltage prevention. *IEEE Transactions on Sustainable Energy* *2*(2), 139–147.
- Wang, X., Y. Pi, W. Mao, and H. Huang (2014). Network coordinated power point tracking for grid-connected photovoltaic systems. *32*(7), 1425.
- Wang, Y., P. Zhang, W. Li, W. Xiao, and A. Abdollahi (2012). Online overvoltage prevention control of photovoltaic generators in microgrids. *IEEE Transaction on Smart Grid* *3*(2), 2071–2078.
- Yang, J., W. Li, T. Chen, W. Xu, and M. Wu (2010). Online estimation and application of power grid impedance matrices based on synchornized phasor measurements. In *IET Generation, Transmission and Distribution*. IEEE.
- Yap, K., T. Huang, Y. Yiakoumis, S. Chinchiali, N. Mckeown, and S. Katti (2013). Scheduling packets over multiple interfaces while respecting user preferences. In *Proceedings of the*

2013 Conference on emerging Networking EXperiments and Technologies, CoNEXT'13. ACM.

Yap, K., N. Mckeown, and S. Katti (2012). Multi-server generalized processor sharing. In *Proceedings of the 24th International Teletraffic Congress.* ACM.

Yoshida, K., K. Kouchi, Y. Nakanishi, H. Ota, and R. Yokoyama (2008). Centralized control of clustered PV generations for loss minimization and power quality. In *IEEE Power and Energy Society General Meeting-Conversion and Delivery of Electrical Energy in the 21st Century*, pp. 1–6. IEEE.